DIRECTION FINDING FOR COHERENT, CYCLOSTATIONARY SIGNALS VIA A UNIFORM CIRCULAR ARRAY

A THESIS SUBMITTED TO
THE GRADUATE SCHOOL OF NATURAL AND APPLIED SCIENCES
OF
MIDDLE EAST TECHNICAL UNIVERSITY

BY

BURCU ATALAY ÇETİNKAYA

IN PARTIAL FULLFILLMENT OF THE REQUIREMENTS
FOR
THE DEGREE OF MASTER OF SCIENCE
IN
ELECTRICAL AND ELECTRONICS ENGINEERING

SEPTEMBER 2009

Approval of the thesis:

DIRECTION FINDING FOR COHERENT, CYCLOSTATIONARY SIGNALS VIA A UNIFORM CIRCULAR ARRAY

submitted by **BURCU ATALAY ÇETİNKAYA** in partial fulfillment of the requirements for the degree of **Master of Science in Electrical and Electronics Engineering Department, Middle East Technical University** by,

Prof. Dr. Canan Özgen _____
Dean, Graduate School of **Natural and Applied Sciences**

Prof. Dr. İsmet Erkmen _____
Head of Department, **Electrical and Electronics Engineering**

Dr. Arzu Tuncay Koç _____
Supervisor, **Electrical and Electronics Engineering Dept., METU**

Examining Committee Members:

Prof. Dr. Yalçın Tanık _____
Electrical and Electronics Engineering Dept., METU

Dr. Arzu Tuncay Koç _____
Electrical and Electronics Engineering Dept., METU

Assoc. Prof. Dr. Sencer Koç _____
Electrical and Electronics Engineering Dept., METU

Asst. Prof. Dr. Çağatay Candan _____
Electrical and Electronics Engineering Dept., METU

Ç. Enis Doyuran (MSc.) _____
ASELSAN Inc.

Date: 11 September 2009

I hereby declare that all information in this document has been obtained and presented in accordance with academic rules and ethical conduct. I also declare that, as required by these rules and conduct, I have fully cited and referenced all material and results that are not original to this work.

Name, Last name : Burcu Atalay Çetinkaya

Signature :

ABSTRACT

DIRECTION FINDING FOR COHERENT, CYCLOSTATIONARY SIGNALS VIA A UNIFORM CIRCULAR ARRAY

Atalay Çetinkaya, Burcu

M. S., Department of Electrical and Electronics Engineering

Supervisor : Dr. Arzu Tuncay Koç

September 2009, 73 pages

In this thesis work, Cyclic Root MUSIC method is integrated with spatial smoothing and interpolation techniques to estimate the direction of arrivals of coherent, cyclostationary signals received via a Uniform Circular Array (UCA). Cyclic Root MUSIC and Conventional Root MUSIC algorithms are compared for various signal scenarios by computer simulations.

A cyclostationary process is a random process with probabilistic parameters, such as the autocorrelation function, that vary periodically with time. Most of the man-made communication signals exhibit cyclostationarity due to the periodicity arising from their carrier frequencies, chip rates, baud rates, etc. Cyclic Root MUSIC algorithm exploits the cyclostationarity properties of signals to achieve signal selective direction of arrival estimation.

Spatial smoothing is presented to overcome the coherent signals problem in a multipath propagation environment. Forward spatial smoothing and forward backward spatial smoothing techniques are investigated. Interpolation method is presented to cope with the restrictions of spatial smoothing on array structure.

Although the array structure that is considered in this thesis (Uniform Circular Array), is not suitable for applying spatial smoothing directly, using interpolation method makes it possible.

Performance of Cyclic Root MUSIC and Conventional Root MUSIC algorithms are compared under variation of various factors by computer simulations. Effects of signal type on the performance of the algorithms are observed by using different signal scenarios.

Key words: Cyclostationarity, Direction Finding, MUSIC, Cyclic MUSIC, Spatial Smoothing, Interpolation

ÖZ

DÜZGÜN DAİRESEL DİZİ KULLANARAK EVREUYUMLU, ÇEVRİMSEL DURAĞAN İŞARETLERLERİN YÖNLERİNİN BULUNMASI

Atalay Çetinkaya, Burcu

Yüksek Lisans, Elektrik Elektronik Mühendisliği Bölümü

Tez Yöneticisi : Dr. Arzu Tuncay Koç

Eylül 2009, 73 sayfa

Bu tez çalışmasında, Düzgün Dairesel Dizi ile alınan evreuyumlu, çevrimsel durağan sinyallerin geliş açısı kestiriminin yapılabilmesi için, uzaysal yumuşatma ve aradeğerlendirme teknikleri Çevrimsel Kök MUSIC yöntemi ile birleştirilmektedir. Bilgisayar benzetimleri ile çeşitli işaret senaryoları için Çevrimsel Kök MUSIC ve Geleneksel Kök MUSIC algoritmaları karşılaştırılmaktadır.

Çevrimsel durağan süreç, özilinti fonksiyonu gibi olasılıksal parametreleri zamana göre periyodik olarak değişen bir gelişigüzel süreçtir. İnsan yapımı haberleşme işaretlerinin bir çoğu taşıyıcı sıklığı, "chip" oranı, sembol hızı gibi parametrelerinden kaynaklanan periyodiklikleri sebebiyle çevrimsel durağanlık içermektedir. Çevrimsel Kök MUSIC algoritması işaret seçici geliş yönü kestirimini sağlayabilmek için sinyallerin çevrimsel durağanlık özelliklerinden faydalanmaktadır.

Çokyollu yayılım ortamlarında gözlenen evreuyumlu işaret probleminin üstesinden gelmek için uzaysal yumuşatma yöntemi sunulmaktadır. İleri uzaysal yumuşatma ve ileri geri uzaysal yumuşatma yöntemleri incelenmektedir. Uzaysal yumuşatma

kullanımının dizi yapısı üzerindeki sınırlamalarının aşılabilmesi için aradeğerlendirme metodu sunulmaktadır. Bu tezde kullanılan Düzgün Dairesel Dizi yapısı doğrudan uzaysal yumuşatma uygulamaya uygun olmamasına rağmen, aradeğerlendirme ile bu mümkün olabilmektedir.

Bilgisayar benzetimleri ile, Çevrimsel Kök MUSIC ve Geleneksel Kök MUSIC algoritmaları çeşitli etkenlerin değişimi altında karşılaştırılmaktadır. Farklı senaryoların kullanımı ile işaret türlerinin algoritmaların performansı üzerindeki etkisi gözlenmektedir.

Anahtar Sözcükler: Çevrimsel durağanlık, Yön Bulma, MUSIC, Çevrimsel MUSIC, Uzaysal Yumuşatma, Aradeğerlendirme

To My Mother and Father

and To Cengiz

ACKNOWLEDGEMENTS

I would like to express my sincere gratitude to my supervisor Dr. Arzu Tuncay Koç for her guidance, advice, criticism, encouragement, endless patience and insight throughout the completion of the thesis.

I would like to express my thanks to all of my friends and colleagues for their support and encouragements.

I am forever indebted to my mother and father who have been supporting me in every aspect of my life.

And lastly, I would like to express my special thanks to my husband Cengiz Çetinkaya for his great support, encouragement, patience and understanding during the completion of this thesis.

TABLE OF CONTENTS

LIST OF TABLES

LIST OF FIGURES

LIST OF ABBREVIATIONS

AM	:	Amplitude Modulation
BPSK	:	Binary Phase Shift Keying
CRB	:	Cramér-Rao Bound
DOA	:	Direction of Arrival
EVD	:	Eigenvalue Decomposition
FBSS	:	Forward Backward Spatial Smoothing
FSS	:	Forward Spatial Smoothing
MUSIC	:	MUltiple SIgnal Classification
RMSE	:	Root Mean Square Error
PAM	:	Pulse Amplitude Modulation
SNR	:	Signal to Noise Ratio
SNOI	:	Signal not of Interest
SOI	:	Signal of Interest
SVD	:	Singular Value Decomposition
UCA	:	Uniform Circular Array
ULA	:	Uniform Linear Array

CHAPTER 1

INTRODUCTION

This thesis is focused on direction of arrival estimation for coherent, cyclostationary signals received via a Uniform Circular Array (UCA). Direction of Arrival (DOA) estimation area of sensor array processing has received considerable amount of interest in the literature during the last few decades. A good survey on DOA estimation subject can be found in [1] and [2]. In [3] exploitation of cyclostationarity properties of the signals has been first introduced into array processing by Gardner to improve the performances of the conventional methods. In the literature several algorithms that exploit cyclostationarity can be found ([4]-[8]). The common drawback of these cyclostationary based and conventional algorithms is their inability to handle coherent (fully correlated) signals in a multipath propagation environment. A preprocessing technique called spatial smoothing for dealing with coherent signals is proposed by Evans et al. and Shan et al. in [9] and in [10], respectively, and further developed in [11] -[13]. The first studies on spatial smoothing method restricted it to Uniform Linear Array (ULA) structures. In [14], Friedlander extended the spatial smoothing method to arbitrary array geometries by combining it with interpolation technique. These researches that combine spatial smoothing and interpolation techniques generally use the conventional eigenvalue based methods for DOA estimation. In this work DOA estimation problem for coherent signals received by a uniformly distributed circular array is combined with cyclostationarity based algorithms. The comparison between the conventional methods and cyclostationarity based methods is considered.

Among the conventional DOA estimation algorithms, MUSIC has been the most widely studied. It is a popular subspace based method and is first derived by Schmidt in [15]. It estimates the DOA of multiple signals arriving at an array of sensors by analyzing the signal subspace structure of the autocorrelation matrix of the received

signal. However, Conventional MUSIC suffers from some drawbacks. It requires that the total number of signals impinging on the array, including both the **S**ignals **o**f **I**nterest (SOIs) and the interference, must be less than the number of sensors ([5]). Another disadvantage of MUSIC that is mentioned in [5] is its inability to resolve two signals spaced more closely than the resolution limit of the array when only one of the signal is a SOI. Additionally while using MUSIC algorithm, the noise characteristics of the sensors and the environment should be known or should be modeled as if the noise is identical and independent from sensor to sensor.

To overcome the above mentioned handicaps of conventional subspace based techniques, cyclostationary based algorithms were proposed ([3]-[6]). While the conventional array processing techniques such as MUSIC basically rely on the spatial properties of the signals impinging on an array of sensors, the proposed methods such as Cyclic MUSIC also exploit the temporal coherency properties of the signals. Temporal coherency appears if the impinging signals are cyclostationary. Many modulated communication signals exhibit a cyclostationarity (or periodic correlation) property, corresponding to the underlying periodicity arising from carrier frequencies or baud rates.

The effects of interferences (background noise and the **S**ignals **n**ot **o**f **I**nterest (SNOIs)) can be eliminated by using Cyclic MUSIC. Cyclic MUSIC also has signal selective property to separate closely spaced signals with different cycle frequencies. This means by the help of Cyclic MUSIC it is possible to resolve two signals spaced more closely than the resolution limit of the array when one of the signals is a SOI and the other is a SNOI ([5]).

Cyclic MUSIC has some disadvantages too. It requires either knowing or measuring frequency parameters, such as carrier frequency or baud rate, to estimate the cyclic autocorrelation matrix. Another requirement is longer observation time for correlation measurements. Additionally, it is necessary to measure a different cyclic autocorrelation matrix for each SOI which has different cyclostationarity properties.

The common drawback for both the Conventional MUSIC and Cyclic MUSIC methods is their inability to handle coherent (fully correlated) signals. Coherent signal issue arises due to multipath propagation. Spatial smoothing technique is

introduced to overcome this fact ([9], [10]). By applying spatial smoothing it is possible not to suffer from this problem under certain conditions.

The most restrictive condition to apply spatial smoothing is to have an array which can be divided into subarrays which all have the same configuration but are shifted with respect to each other, i.e., Uniform Linear Array. To generalize the spatial smoothing method to arbitrary array configurations, interpolation technique may be performed ([14]).

In this thesis, Cyclic MUSIC method is integrated with spatial smoothing and interpolation to estimate the DOA's of coherent, cyclostationary signals received via a Uniform Circular Array (UCA). Cyclic MUSIC is compared with Conventional MUSIC for this signal scenario. The organization of this thesis is as follows: A general review of cyclostationarity concept and basic definitions are given in Chapter 2. In Chapter 3, Cyclic MUSIC, spatial smoothing, interpolation and the implementation of these techniques together are explained in detail, preceded by modeling and the formulation of problem. In Chapter 4, the simulation results for the performance analysis and comparison for Conventional MUSIC and Cyclic MUSIC methods are given. The last chapter includes the conclusion.

Throughout this thesis, following notation is used:

$[.]^T$: Transpose

$[.]^H$: Complex Conjugate Transpose

$[.]^*$: Complex Conjugate

$E\{.\}$: Expectation, an ensemble average operator

$\langle . \rangle$: Infinite Time Average such that $\langle . \rangle \triangleq \lim_{T \to \infty} \frac{1}{T} \int_{-T/2}^{T/2} (.) dt$

CHAPTER 2

CYCLOSTATIONARY SIGNALS

This section includes a brief discussion for cyclostationarity concept and gives basic properties and definitions for cyclostationary signals.

Stated simply, a process exhibits cyclostationarity if its statistics, such as mean and autocorrelation function, vary periodically with time.

Classical dice-rolling example that is used so much in statistics can also help to understand the cyclostationarity concept better ([16]). If a fair, six-sided die is rolled a thousand times every day, then same mean score, i.e., 3.5, would be expected for each day. Since the statistics do not vary with time, this process is called stationary. To make the similar experiment for cyclostationarity concept, two dice can be considered. One of the dice should have six sides, and the other should have nine sides. If six sided-die is rolled on Mondays, Tuesdays, Wednesdays, and Thursdays and the nine-sided die for the rest of the week, then a mean of 3.5 on the days where six-sided die is used, and a mean of 5 on the days where nine-sided die is used would be expected. Therefore, the statistics do vary with time periodically (i.e., weekly), and the process is said to be cyclostationary.

Cyclostationary signal model is applicable for most of the man-made communication signals. Although many conventional statistical signal processing methods treat random signals as if they are statistically stationary, parameters of the most man-made signals encountered in communication, radar and sonar systems do vary periodically with time so these signals can be modeled as cyclostationary processes. In some cases even multiple periodicities, which are not harmonically related, are involved. Examples of the underlying reasons of this periodic fluctuation in statistics can be cited as the sinusoidal carriers in amplitude, phase, and frequency modulation systems, periodic keying of the amplitude, phase or frequency in digital modulation

systems, chip rates used in spread spectrum signals, and some radar systems ([17]-[19]).

A more formal description of cyclostationarity is given as the property that enables spectral line generation with some type of quadratic time-invariant transformation by Gardner in [17]. Cyclostationarity is characterized by the cyclic autocorrelation function, which is a generalization of the conventional autocorrelation function.

2.1 SPECTRAL LINE GENERATION

In this section, a summary of spectral line generation property which is described exhaustively in [17] is given.

Assume a signal, $x(t)$, which contains a finite strength additive sine wave component with frequency α as follows:

$$a\cos(2\pi\alpha t+\theta) \quad \text{with } \alpha \neq 0 \tag{2.1}$$

The Fourier coefficient of this signal can be calculated as

$$M_x^\alpha = \left\langle x(t)e^{-j2\pi\alpha t}\right\rangle = \frac{1}{2}ae^{j\theta} \tag{2.2}$$

where $\langle . \rangle$ denotes infinite-time average, i.e.,

$$M_x^\alpha = \lim_{T\to\infty}\frac{1}{T}\int_{-T/2}^{T/2} x(t)e^{-j2\pi\alpha t}dt \tag{2.3}$$

Since this Fourier coefficient has a nonzero value, the power spectral density (PSD) of $x(t)$ includes a spectral line at frequency $f=\alpha$ and its image $f=-\alpha$, i.e., PSD of $x(t)$ contains an additive component as follows:

$$\left|M_x^\alpha\right|^2\left[\delta(f-\alpha)+\delta(f+\alpha)\right] \tag{2.4}$$

where $\delta(.)$ is the Dirac delta, or impulse, function.

It is said that such a signal exhibits *first order periodicity*.

$x(t)$ can be considered as the summation of the finite strength additive sine wave component in (2.1) and a residual part, $n(t)$

$$x(t) = a\cos(2\pi\alpha t + \theta) + n(t) \tag{2.5}$$

where $n(t)$ is defined to be the component which is left after subtraction of (2.1) from $x(t)$. It is assumed that $n(t)$ is random. Here, the word random is used to mean nothing more than the indistinct behavior. If the sine wave component of the signal is weaker than this residual, it might be more difficult to observe the periodicity of $x(t)$. In such situations, it is said that the signal contains *hidden periodicity*. However, in such cases it is still possible to detect the periodicity by searching for the related spectral lines.

In hidden periodicity cases, it is sometimes possible to observe the spectral lines of the PSD after a time-invariant transformation. For example a squarer can be used as a transformation.

An example of this operation can be observed on a pulse-amplitude modulated (PAM) signal.

$$x(t) = \sum_{n=-\infty}^{\infty} a(nT_0)\,p(t - nT_0) \tag{2.6}$$

where $p(t)$ is a pulse whose width is less than interpulse time (See Figure 1).

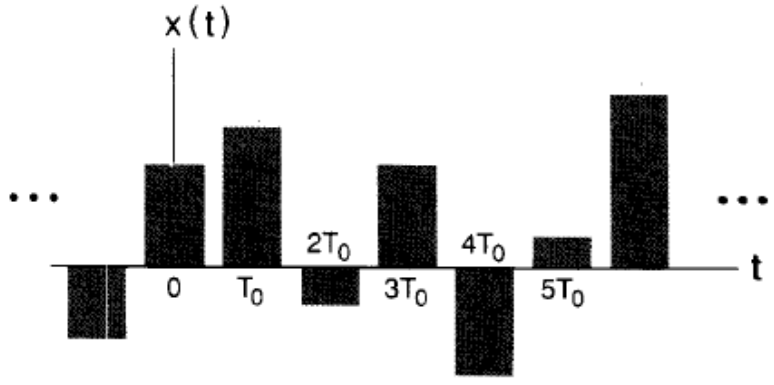

Figure 1 A PAM signal with pulse width less than interpulse time

The PSD of $x(t)$ can be calculated as follows:

$$S_x(f) = \frac{1}{T_0}\left|P(f)\right|^2 \sum_{m=-\infty}^{\infty} S_a(f - m/T_0) \tag{2.7}$$

The PSD's of $a(t)$ and $x(t)$, $S_a(f)$ and $S_x(f)$, are given in Figure 2-a and Figure 2-b. As can be seen from the figure no spectral line exists in the PSDs, regardless of the periodic repetition of the pulses in $x(t)$.

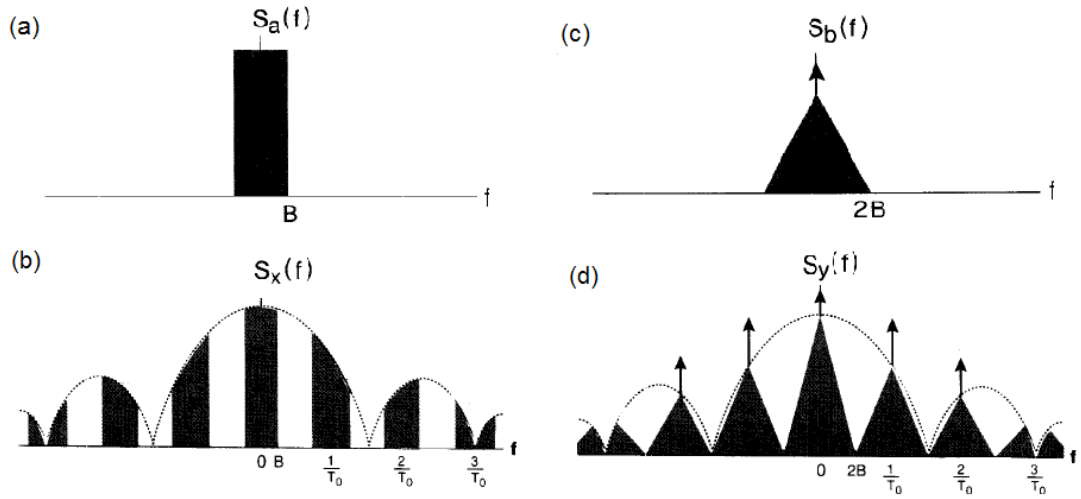

Figure 2 (a) PSD of $a(t)$, $S_a(f)$ **(b)** PSD of the PAM signal, $S_x(f)$ **(c)** PSD of $b(t)$, $S_b(f)$ **(d)** PSD of the squared PAM signal, $S_y(f)$

To detect the spectral lines, square of $x(t)$ should be inspected.

$$y(t) = x^2(t) = \sum_{n=-\infty}^{\infty} b(nT_0)q(t - nT_0) \tag{2.8}$$

where

$$b(nT_0) = a^2(nT_0) \tag{2.9}$$

and where

$$q(t) = p^2(t) \tag{2.10}$$

Then, PSD of $y(t)$ can be calculated as follows:

$$S_y(f) = \frac{1}{T_0}|Q(f)|^2 \sum_{m=-\infty}^{\infty} S_b(f - m/T_0) \tag{2.11}$$

where $Q(f)$ is the Fourier transform of $q(t)$. As can be seen from Figure 2-c and Figure 2-d, $S_b(f)$ has spectral line at $f = 0$, so $S_y(f)$ has also spectral lines at the multiples of pulse rate, $1/T_0$.

This means that the hidden periodicity in this PAM signal is discovered after the squaring transformation.

2.2 THE CYCLIC AUTOCORRELATION FUNCTION

For some cases, the above mentioned squaring transformation does not work and a different quadratic transformation involving delays can be required to observe the hidden periodicity ([17]). For example, for a PAM signal in which $p(t)$ is a flat pulse with height 1 and pulse width T_0 (Figure 3), no spectral line in PSD can be observed after squaring transformation.

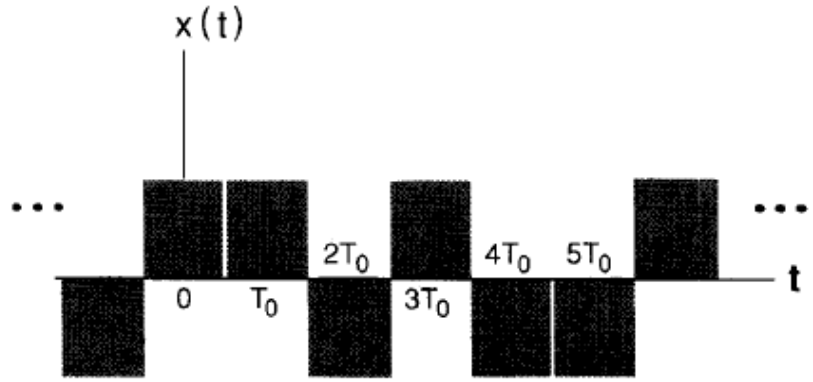

Figure 3 A PAM signal with full duty cycle and flat pulse height

However, using such a transformation:

$$y(t) = x(t)x(t-\tau) \tag{2.12}$$

for nonzero delays τ, spectral lines at multiples of pulse rate, $1/T_0$, can be obtained.

This means, $y(t)$ has nonzero Fourier coefficients.

$$M_y^{\alpha} = \left\langle y(t)e^{-j2\pi\alpha t} \right\rangle = \left\langle x(t)x(t-\tau)e^{-j2\pi\alpha t} \right\rangle \neq 0 \tag{2.13}$$

Therefore, its PSD includes spectral lines at frequencies $\alpha = m/T_0$, for some integers m.

Definition of *second order periodicity* or *cyclostationarity* is based on (2.12) and (2.13). The signal exhibits cyclostationarity if and only if the PSD of the delay

product signal (2.12) for some delays τ contains spectral lines at some nonzero frequencies $\alpha \neq 0$. That is to say, cyclostationary signals should satisfy (2.13).

Sometimes it is more convenient to work with the symmetric delay product:

$$y(t) = x(t + \tau / 2)x^*(t - \tau / 2) \tag{2.14}$$

For the Fourier coefficient in (2.13), another notation can also be used, namely $R_x^\alpha(\tau)$, since it returns to conventional autocorrelation function when $\alpha = 0$.

$$R_x^\alpha(\tau) \triangleq \left\langle x(t + \tau / 2)x^*(t - \tau / 2)e^{-j2\pi\alpha t} \right\rangle \tag{2.15}$$

Furthermore, since $R_x^\alpha(\tau)$ is a generalization of the autocorrelation function, in which a cyclic (sinusoidal) weighting factor is included before the time averaging is carried out, $R_x^\alpha(\tau)$ is called the *cyclic autocorrelation function*. Additionally, any nonzero value of the frequency parameter α for which $R_x^\alpha(\tau) \neq 0$ is called *cycle frequency* and the delay τ is called *lag* parameter.

In order to select the cycle frequency and lag parameters correctly, cyclic autocorrelation function can be observed under varying values of α and τ. In this section, cyclic autocorrelation functions of four different signal types are depicted by using varying values of α and τ. Three of the selected signals are BPSK modulated ones which have different bit rates and one of the signals is AM.

The carrier frequency of the signals are 10 MHz. They are sampled with 32 MHz frequency during $25\mu s$. The bit rates of the BPSK signals are selected as 4, 3.2, and 8 Mb/s. AM signal has 50% modulation depth.

The cyclic autocorrelation functions of these signals are examined here since they belong to the signal scenarios that are used in the simulations whose results are discussed in Chapter 4. Generation of these signals is also given in a detailed manner in Chapter 4.

In Figure 4, magnitude of the cyclic autocorrelation function is estimated for a $4Mb/s$ BPSK modulated signal. Figure 5 shows two dimensional version of this graph to observe the cycle frequency and time lag parameters easier. As can be seen from these figures, there are more than one peak values of cyclic autocorrelation

function corresponding to different α values. In [17], the cyclic properties of a BPSK modulated signal are analyzed and it is shown that a BPSK signal has its cycle frequencies in $\alpha = \pm 2f_0 + m/T_0$ and $\alpha = m/T_0$ for integer m, where f_0 is the carrier frequency of the signal and $1/T_0$ is equal to the bit rate of the signal. Throughout these candidates, the main cycle frequency of the signal can be selected as equal to the bit rate of the signal, $4MHz$, where the cyclic autocorrelation function has its maximum value. In this maximum value the time lag parameter, τ is equal to $0.125\mu s$.

Figure 6-Figure 9 show cyclic autocorrelation function of BPSK signals with different bit rates, $3.2Mb/s$ and $8Mb/s$. As can be observed from these figures, the cyclic autocorrelation function has its maximum value also in the cycle frequencies that are equal to the bit rates of the BPSK signals.

Figure 10 and Figure 11 show the cyclic autocorrelation function of an AM signal. These figures are included to show that this AM signal does not exhibit cyclostationarity characteristics in the cycle frequencies which coincide with the cycle frequencies of the selected BPSK modulated signals. In [17], it is shown that an AM signal has its cycle frequencies where $\alpha = \pm 2f_0$ and $\alpha = 0$.

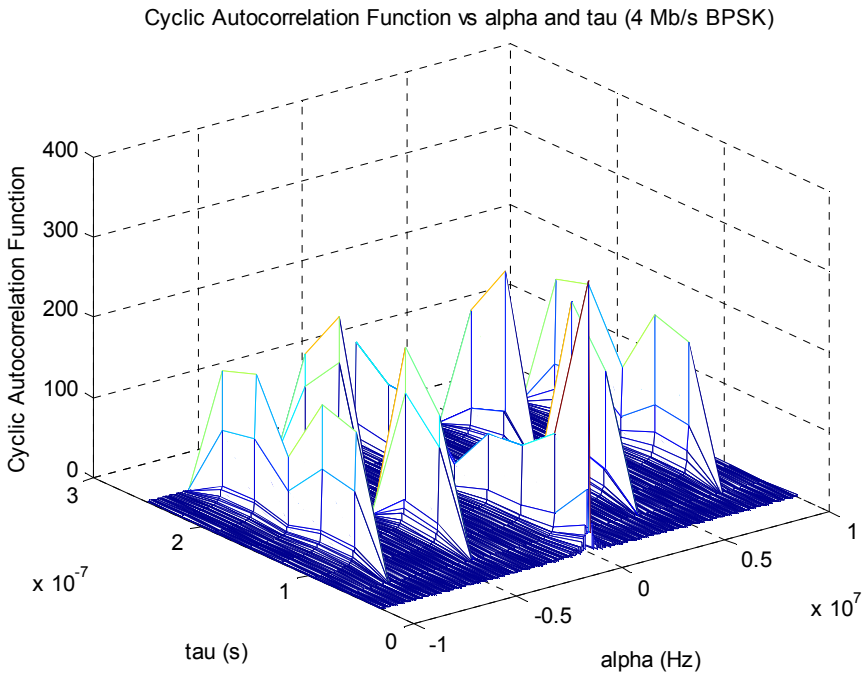

Figure 4 Magnitude of the cyclic autocorrelation function ($R^{\alpha}(\tau)$) versus cycle frequency (α) and lag (τ) for a BPSK signal which has $4Mb/s$ bit rate.

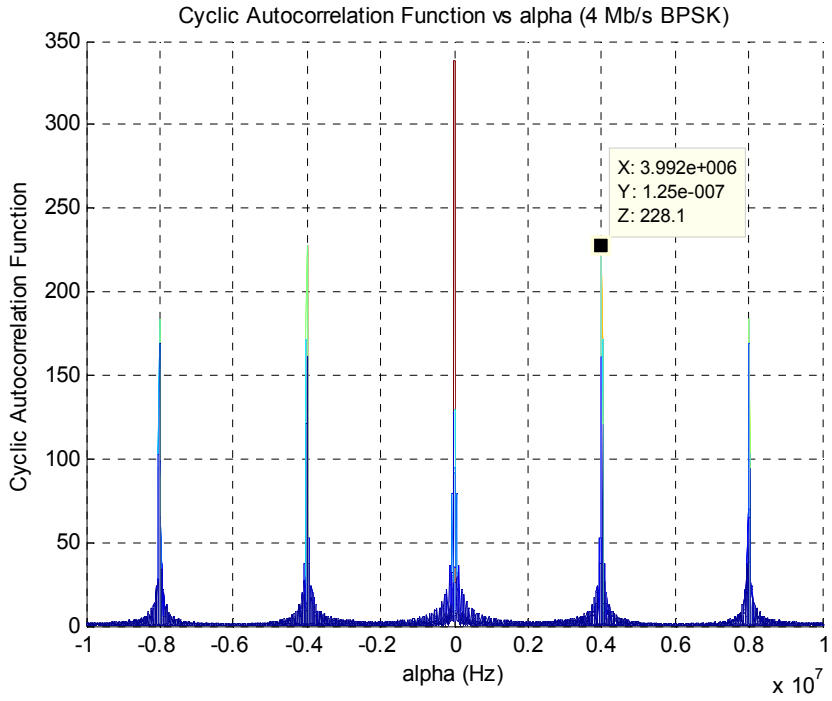

Figure 5 Magnitude of the cyclic autocorrelation function ($R^{\alpha}(\tau)$) versus cycle frequency (α) for a BPSK signal which has $4Mb/s$ bit rate.

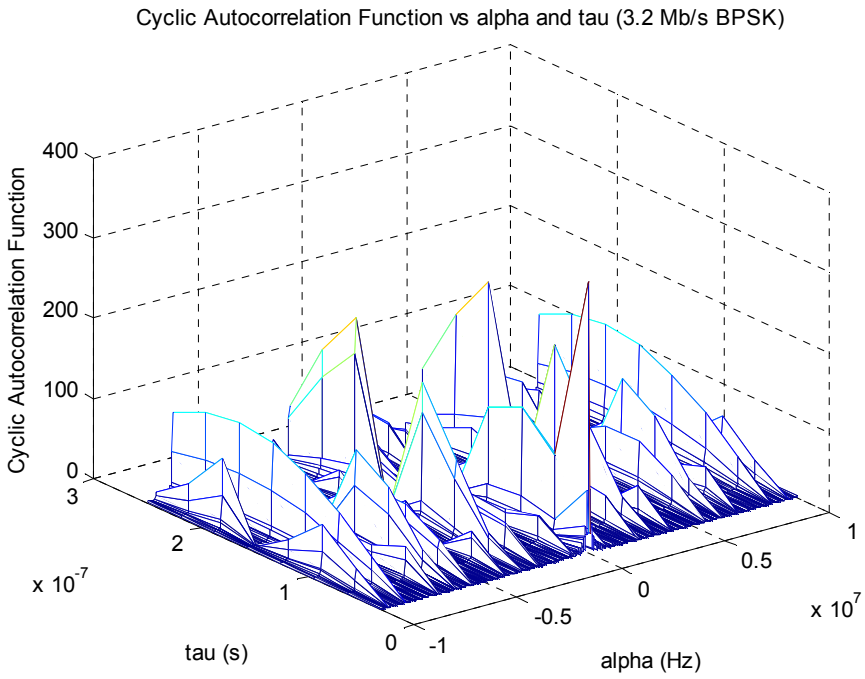

Figure 6 Magnitude of the cyclic autocorrelation function ($R^{\alpha}(\tau)$) versus cycle frequency (α) and lag (τ) for a BPSK signal which has $3.2Mb/s$ bit rate.

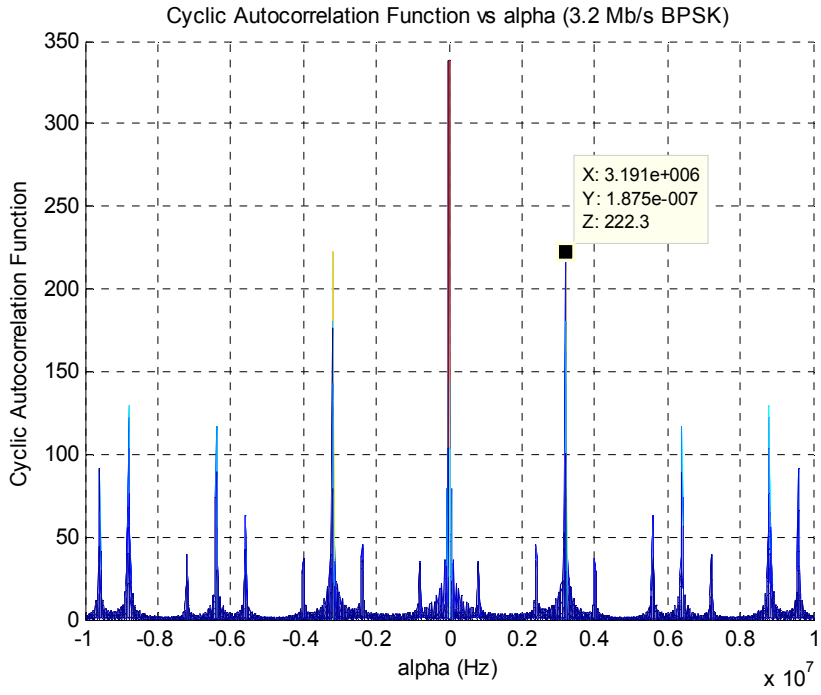

Figure 7 Magnitude of the cyclic autocorrelation function ($R^{\alpha}(\tau)$) versus cycle frequency (α) for a BPSK signal which has $3.2Mb/s$ bit rate.

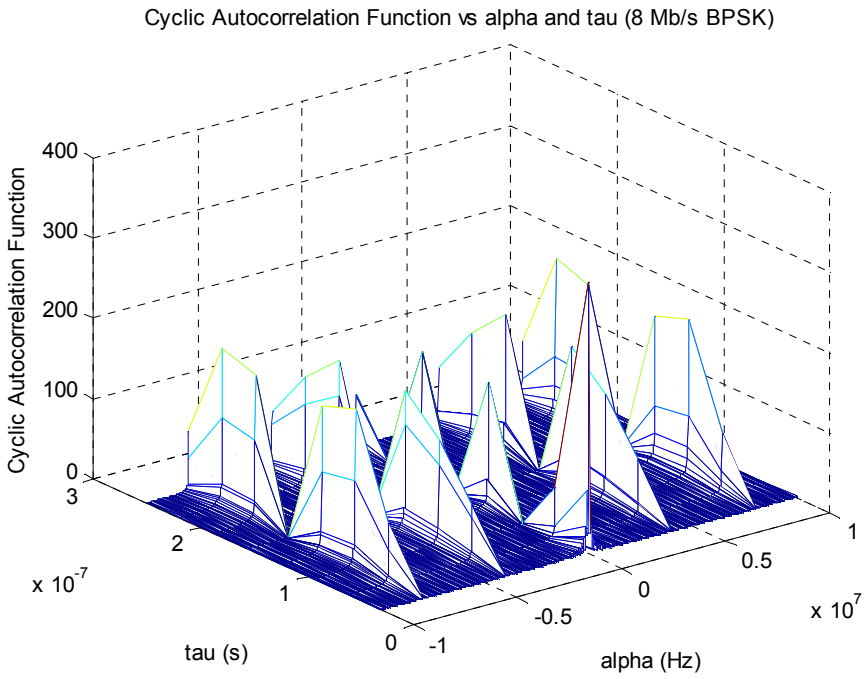

Figure 8 Magnitude of the cyclic autocorrelation function ($R^{\alpha}(\tau)$) versus cycle frequency (α) and lag (τ) for a BPSK signal which has $8Mb/s$ bit rate.

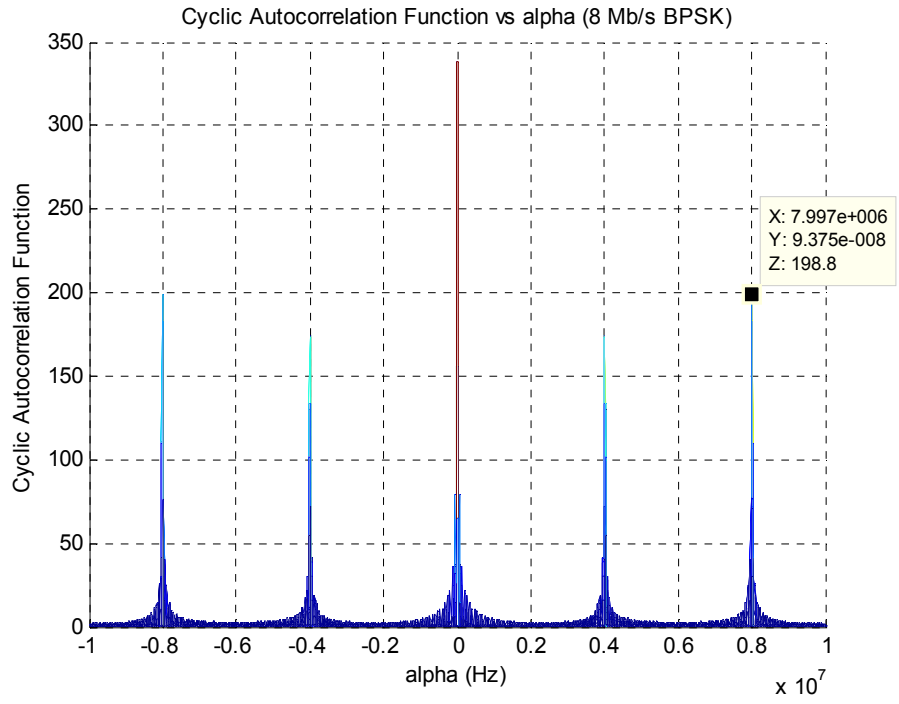

Figure 9 Magnitude of the cyclic autocorrelation function ($R^{\alpha}(\tau)$) versus cycle frequency (α) for a BPSK signal which has $8Mb/s$ bit rate.

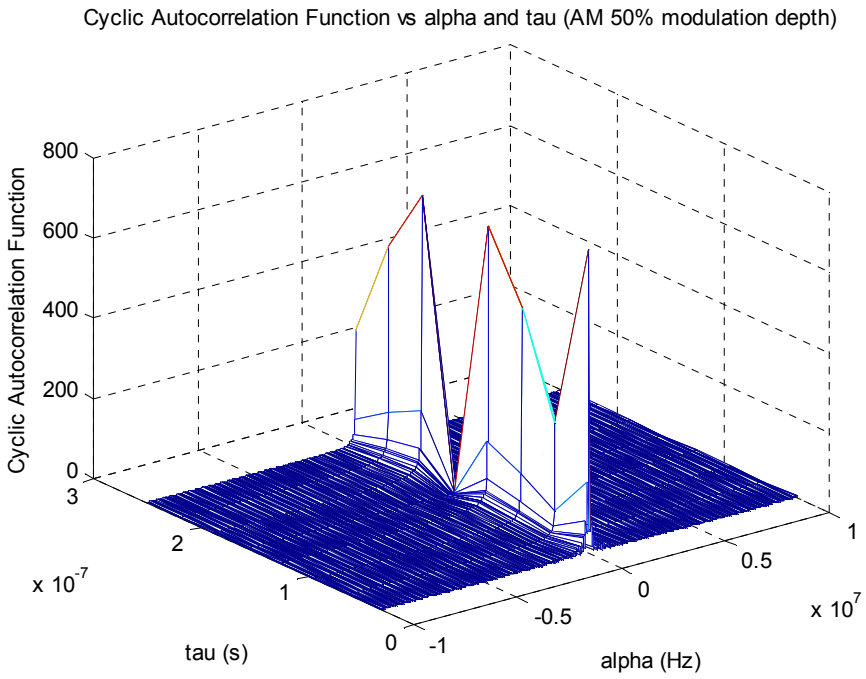

Figure 10 Magnitude of the cyclic autocorrelation function ($R^{\alpha}(\tau)$) versus cycle frequency (α) and lag (τ) for an AM signal.

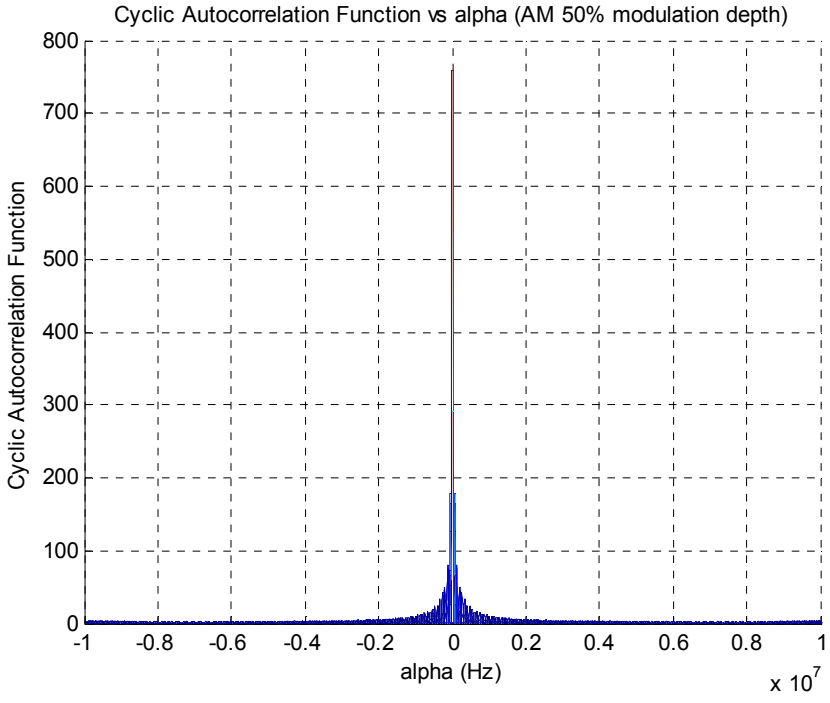

Figure 11 Magnitude of the cyclic autocorrelation function ($R^{\alpha}(\tau)$) versus cycle frequency (α) for an AM signal.

CHAPTER 3

THE DF ALGORITHM

In this chapter, the problem of estimating the DOAs of cyclostationary signals is investigated. Some of the incoming signals are assumed to be fully correlated and the signals are assumed to be received with a UCA. Initially the assumptions used for problem formulation are stated, and appropriate models for the signal and noise are developed. Then the Conventional Root MUSIC and Cyclic Root MUSIC methods are discussed. To solve the coherency between the impinging signals spatial smoothing technique is explained. Afterwards, the required preprocessing for spatial smoothing, namely, interpolation is discussed. Then implementation of these techniques together is explained in detail.

3.1 SIGNAL MODEL

Consider a UCA with M sensors. Suppose that N electromagnetic waves impinge on this array from angular directions $\{\theta_1,\ldots,\theta_N\}$ as in Figure 12.

The received signal at the mth sensor can be expressed as

$$r_m(t) = \sum_{n=1}^{N} a_{mn} s_n(t) e^{j\pi(x_m \sin\theta_n + y_m \cos\theta_n)} + n_m(t) \tag{3.1}$$

where $s_n(t)$ is the signal for the nth wavefront, a_{mn} is the response of the m th sensor to the n th wavefront, (x_m, y_m) are the coordinates of the m th sensor measured in half wave-length units, $n_m(t)$ is the additive noise at the m th sensor. The noise is assumed to be uncorrelated with the signals and uncorrelated from sensor to sensor and to have variance σ^2.

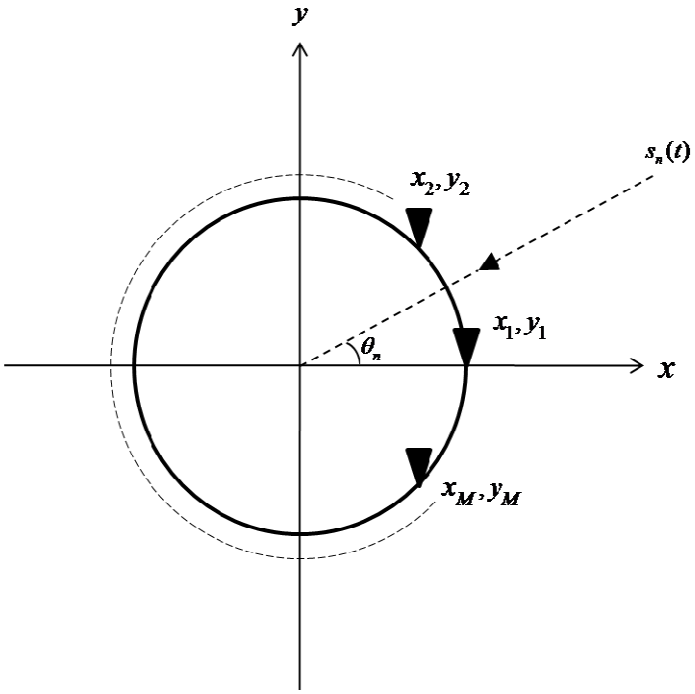

Figure 12 M-element Uniform Circular Array Structure

Rewriting (3.1) in vector notation, assuming the sensors are omnidirectional, such that $a_{mn} = 1$, received signal can be obtained as

$$r(t) = \sum_{n=1}^{N} a(\theta_n) s_n(t) + n(t) \tag{3.2}$$

where $r(t)$ is an $Mx1$ vector for the received signal,

$$r(t) = \left[r_1(t), \ldots, r_M(t) \right]^T \tag{3.3}$$

and $a(\theta_n)$ is an $Mx1$ steering vector of the array for the signal from the direction θ_n,

$$a(\theta_n) = \left[e^{j\pi(x_1 \sin\theta_n + y_1 \cos\theta_n)}, \ldots, e^{j\pi(x_M \sin\theta_n + y_M \cos\theta_n)} \right]^T \tag{3.4}$$

and $n(t)$ is an $Mx1$ vector for the received noise.

(3.2) can be simplified as follows:

$$r(t) = AS(t) + n(t) \tag{3.5}$$

where $S(t)$ is the $Nx1$ vector for the incoming signal,

$$S(t) = \left[s_1(t), \ldots, s_N(t)\right]^T \tag{3.6}$$

and A, the array manifold matrix, is the MxN matrix.

$$A = \left[a(\theta_1), \ldots, a(\theta_N)\right] \tag{3.7}$$

3.2 CONVENTIONAL ROOT MUSIC

In this section Conventional Root MUSIC algorithm, that is the most widely studied DOA estimation method among the subspace based array processing techniques, is summarized. MUSIC is first derived by Schmidt in [15]. It utilizes the signal subspace structure of the conventional autocorrelation matrix of the received signal to estimate the DOAs of incoming signals.

Conventional autocorrelation matrix for $r(t)$ is an MxM matrix and can be defined as follows:

$$R = E\{r(t)r(t)^H\} = AR_S A^H + \sigma^2 I \tag{3.8}$$

where R_s is conventional signal autocorrelation matrix,

$$R_S = E\{S(t)S(t)^H\} \tag{3.9}$$

and σ^2 is noise variance, I is an MxM identity matrix.

Note that R_s is:

- *Diagonal* and *nonsingular* when signals are *uncorrelated*.
- *Nondiagonal* and *nonsingular* when signals are *partially correlated*.
- *Nondiagonal* and *singular* when signals are *fully correlated (coherent)*.

Eigenvalues and the corresponding eigenvectors of R may be denoted by

$$\{\lambda_1 \geq \lambda_2 \geq \ldots \geq \lambda_M\} \text{ and } \{v_1, v_2, \ldots, v_M\} \tag{3.10}$$

When R_s is nonsingular (signals are not coherent or partially correlated), the rank of $AR_s A^H$ will be N and the following properties will be applicable.

1. The minimum eigenvalue of R is equal to σ^2 with multiplicity $M-N$

$$\lambda_{N+1} = \lambda_{N+2} = \ldots = \lambda_M = \sigma^2 \tag{3.11}$$

2. The eigenvectors corresponding to the minimal eigenvalues, namely E_n, are orthogonal to the columns of the matrix A

$$\{v_{N+1}, \ldots, v_M\} \perp \{a(\theta_1), \ldots, a(\theta_N)\} \tag{3.12}$$

The Conventional MUSIC algorithm and other subspace based methods exploit the above given properties; (3.11) and (3.12).

There are two popular way of implementing the Conventional MUSIC method; Spectral MUSIC and Root MUSIC. Root MUSIC will be preferred in this study, since it does not require a computationally intensive search procedure for DOA estimation as in Spectral MUSIC. Moreover, it often has a better performance than Spectral MUSIC, [20].

Disadvantage of Root MUSIC is the limitation on array geometry. The array manifold matrix should have Vandermonde structure to apply Root MUSIC. This means a ULA is required for Root MUSIC method [21].

For a ULA given in Figure 13, steering vector in (3.4) can be rewritten as

$$a(\theta_n) = \left[e^{j\pi(x_1 \sin\theta_n)}, \ldots, e^{j\pi(x_M \sin\theta_n)} \right]^T \tag{3.13}$$

where

$$\begin{bmatrix} x_1 & x_2 & \cdots & x_M \end{bmatrix}^T = d \left[-\frac{(M-1)}{2} \quad 1-\frac{(M-1)}{2} \quad \cdots \quad \frac{(M-1)}{2} \right]^T \tag{3.14}$$

and d is the distance between adjacent sensors.

Using (3.13) and (3.14) together, steering vector can be obtained as

$$a(\theta_n) = e^{j\pi d \sin\theta_n [-\frac{M-1}{2} \quad 1-\frac{M-1}{2} \quad \cdots \quad \frac{M-1}{2}]^T} \tag{3.15}$$

Rewriting it in $e^{-j\pi\left(\frac{M-1}{2}\right)d\sin\theta_n}$ parenthesis, the following expression is obtained.

$$a(\theta_n) = e^{-j\pi(\frac{M-1}{2})d\sin\theta_n} [1 \quad e^{j\pi d\sin\theta_n} \quad \cdots \quad e^{j(M-1)\pi d\sin\theta_n}]^T \tag{3.16}$$

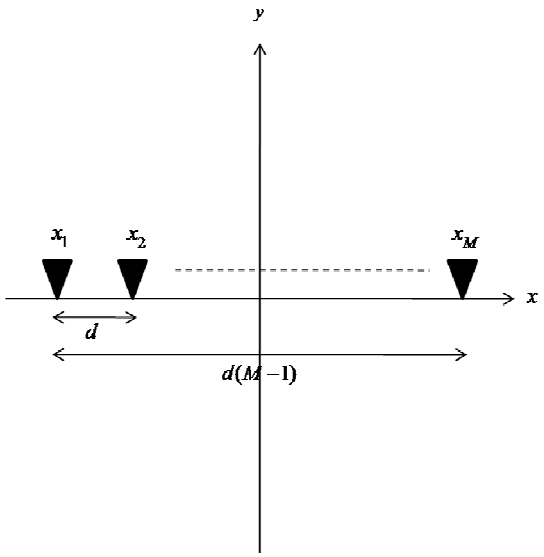

Figure 13 M-element Uniform Linear Array Structure

Substituting $\phi = \pi d \sin\theta_n$, array steering vector is obtained as follows:

$$a(\phi) = e^{-j(\frac{M-1}{2})\phi}[1 \quad e^{j\phi} \quad \cdots \quad e^{j(M-1)\phi}]^T \tag{3.17}$$

By putting $z = e^{j\phi}$ in the steering vector, the following expression is obtained.

$$a(z) = z^{-\frac{M-1}{2}}[1 \quad z \quad \cdots \quad z^{M-1}]^T \tag{3.18}$$

By using the properties given in (3.11) and (3.12), the polynomial required for Root MUSIC can be written as follows:

$$\mathbb{Q}(z) = a(1/z)^T E_n E_n^H a(z) = 0 \tag{3.19}$$

where E_n is noise subspace that consists of eigenvectors corresponding to the minimal eigenvalues.

The roots of the polynomial in (3.19) are the candidates for the solution of z. Due to the conjugate symmetry of the polynomial $\mathbb{Q}(z)$, its roots come in pairs where one root is the conjugate reciprocal of the other. Only one of each of these pairs should be selected.

After selecting N roots closest to the unit circle, it is easy to find the direction of arrival of the N signals from the selected roots as follows:

$$\phi = \arg(z) \tag{3.20}$$

$$\theta_n = \frac{\arcsin \phi}{\pi d} \tag{3.21}$$

In practice, to use the above explained Root MUSIC method, if a set of snapshots of the received signal $\{r(t), t = 1, \ldots, T_{obs}\}$ is given, autocorrelation matrix may be estimated as ([15] and [22])

$$\hat{R} = (1/T_{obs}) \sum_{t=1}^{T_{obs}} r(t) r^H(t) \tag{3.22}$$

3.3 CYCLIC ROOT MUSIC

In this section, a signal selective DOA estimation algorithm, namely, Cyclic MUSIC, is presented. Cyclic MUSIC is first derived by Gardner in [3] to exploit the cyclostationarity property of the signals to improve the performances of the conventional methods. It is further developed by other researchers in [4]-[8]. Instead of using just spatial properties of sources to estimate the DOA, these algorithms also utilize the spectral coherence properties.

Main difference between Conventional Root MUSIC and Cyclic Root MUSIC is that; Conventional Root MUSIC estimates the DOAs of the sources by using the conventional autocorrelation matrix, whereas Cyclic Root MUSIC requires the estimation of the cyclic autocorrelation matrix that reflects the cyclostationarity of incoming signals.

Assume that among the N electromagnetic waves impinging on the array, K of them have spectral correlation with a certain cycle frequency α and a time lag τ and remaining I of them do not exhibit any cyclostationarity properties or exhibit cyclostationarity with different cycle frequencies. The aim is to find the DOAs of that K signals (SOIs), while eliminating I interferers (SNOIs) and background noise.

The cyclic autocorrelation matrix of the received signal can be calculated with the following equation as defined in Chapter 2.

$$R^{\alpha}(\tau) = \left\langle r(t+\tau/2) r^{H}(t-\tau/2) e^{-j2\pi\alpha t} \right\rangle \tag{3.23}$$

where $r(t)$ is an $Mx1$ vector as described in (3.5).

Simplifying (3.23), following equation can be obtained ([5])

$$R^{\alpha}(\tau) = A R_{s}^{\alpha}(\tau) A^{H} \tag{3.24}$$

where

$$R_{s}^{\alpha}(\tau) = \left\langle S(t+\tau/2) S^{H}(t-\tau/2) e^{-j2\pi\alpha t} \right\rangle \tag{3.25}$$

and $S(t), A$ are as given in (3.6), (3.7), respectively.

The Cyclic Root MUSIC algorithm can be implemented as follows:

1. Select the cycle frequency α and the time lag τ parameters for the SOIs whose DOAs are desired to be found as described in Chapter 2.
2. Compute the cyclic autocorrelation matrix of the received signal, $R^{\alpha}(\tau)$, by using the selected α and τ values.
3. Perform EVD to find the noise subspace E_n. Note that for nonsingular $R_{s}^{\alpha}(\tau)$, the rank of $R^{\alpha}(\tau)$ will be equal to number of SOIs (K) ([5]). Therefore E_n will consist of eigenvectors corresponding to the $M-K$ minimal eigenvalues.

After finding E_n, the remaining parts of the Cyclic Root MUSIC can be implemented similarly as in the Conventional Root MUSIC by using (3.13)- (3.21). However the selected roots will only give the direction of arrivals of SOIs. Therefore, Cyclic Root MUSIC is known as a signal selective method.

In practice, given a set of snapshots of the received signal $\{r(t), t = 1, \ldots, T_{obs}\}$ cyclic autocorrelation matrix can be estimated as follows [6]:

$$\widehat{R^{\alpha}}(\tau) = (1/T_{obs}) \sum_{t=1}^{T_{obs}} r(t+\tau/2) r^{H}(t-\tau/2) e^{-j2\pi\alpha t} \tag{3.26}$$

3.4 SPATIAL SMOOTHING

Coherent signals that appear in the multipath propagation environments causes unsatisfactory performance in the application of both Conventional Root MUSIC and Cyclic Root MUSIC. In this section, the spatial smoothing preprocessing method is examined to cope with coherent signals. This method was first introduced in [9] and [10] and further developed in [11].

As stated in Section 3.2 and Section 3.3, the ranks of R_s and $R_s^{\alpha}(\tau)$ are N and K, respectively for uncorrelated signal scenarios. In the case of coherency, conventional autocorrelation matrix or cyclic autocorrelation matrix will be rank deficient; in other words the ranks of R_s and $R_s^{\alpha}(\tau)$ are less than N and K. In such a situation Conventional Root MUSIC and Cyclic Root MUSIC algorithms cannot be used directly. Therefore, spatial smoothing is required to be applied to the autocorrelation matrices at first.

In this section the spatial smoothing is only discussed for conventional autocorrelation matrix. However in the following sections of this thesis, steps to apply spatial smoothing on cyclic autocorrelation matrix will also be included.

Assume that two SOIs, $s_1(t)$ and $s_2(t)$, are linearly dependent, e.g.,

$$s_2(t) = \beta s_1(t) \tag{3.27}$$

where β is a complex scalar that describes the correlation between signals.

Then the received signal expression in (3.5) can be rewritten as follows:

$$r(t) = \widetilde{A}\widetilde{S}(t) + n(t) \tag{3.28}$$

where

$$\widetilde{S}(t) = [s_1(t) + \beta s_1(t), s_3(t), \cdots, s_N(t)] \tag{3.29}$$

$$\widetilde{A} = [a(\theta_1) + \beta a(\theta_2), a(\theta_3), \cdots, a(\theta_N)] \tag{3.30}$$

Then (3.8) becomes

$$R = \widetilde{A}\widetilde{R}_s\widetilde{A}^H + \sigma^2 I \tag{3.31}$$

where

$$\widetilde{R_s} = E\{\tilde{S}(t)\tilde{S}(t)^H\} \tag{3.32}$$

$\widetilde{R_s}$ is still nonsingular and the columns of $\tilde{A}$ are linearly independent. Therefore, it is only possible to estimate the direction of arrivals of remaining SOIs correctly. However, it is not possible to estimate the DOAs of coherent SOIs, θ_1 and θ_2.

Spatial smoothing is a preprocessing to make R_s nonsingular again even the signals are coherent and serves to estimate the DOAs of coherent signals. The formulation of spatial smoothing is summarized in the following.

For spatial smoothing a ULA with size M is divided into overlapping L subarrrays of size M_0 as shown in Figure 14.

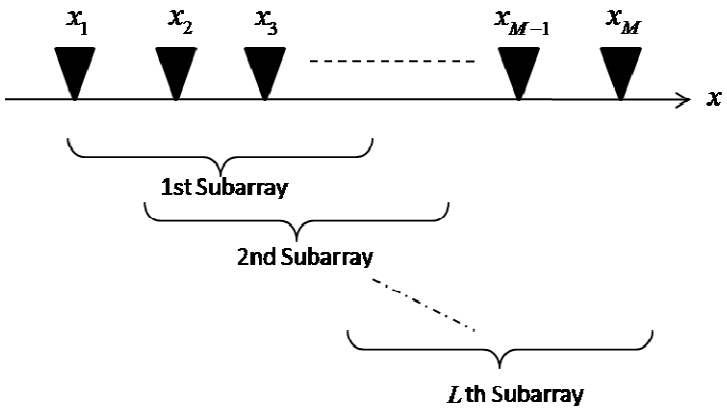

Figure 14 Division of an M-element ULA into Subarrays for Forward Spatial Smoothing

The subarray number is

$$L = M - M_0 + 1 \tag{3.33}$$

The received signal by the lth subarray can be expressed as

$$r_l(t) = AD_lS(t) + n_l(t) \tag{3.34}$$

where D_l denotes an NxN diagonal matrix

$$D_l = diag\{e^{j\pi d(l-1)\sin\theta_1},\ldots,e^{j\pi d(l-1)\sin\theta_N}\} \tag{3.35}$$

and A is the array manifold of the subarray (Note that previously A was used for the array manifold of the full array. Here, for the sake of simplicity the manifold of the subarray is also given by same notation).

The autocorrelation matrix of the received signal by the lth subarray can be denoted as

$$R_l = AD_lR_sD_l^HA^H + \sigma^2 I \tag{3.36}$$

The spatially smoothed autocorrelation matrix is the average of the subarrays' autocorrelation matrices

$$\overline{R} = \frac{1}{L}\sum_{l=1}^{L} R_l \tag{3.37}$$

Substituting (3.36) into (3.37), below equation is obtained

$$\overline{R} = A(\frac{1}{L}\sum_{l=1}^{L} D_lR_sD_l^H)A^H + \sigma^2 I \tag{3.38}$$

Then, (3.38) can be simplified as

$$\overline{R} = A\overline{R_s}A^H + \sigma^2 I \tag{3.39}$$

where

$$\overline{R_s} = \frac{1}{L}\sum_{l=1}^{L} D_lR_sD_l^H \tag{3.40}$$

It is shown that if the number of subarrays is equal to or greater than the number of the impinging signals ($L > N$), then it is guaranteed that $\overline{R_s}$ is nonsingular even there are coherent signals. Therefore, regardless of the coherency between signals it is possible to apply standard subspace algorithms on this smoothed autocorrelation matrix that exactly has the same form as R ([9]-[11]). The proof of this nonsingularity condition is given in Appendix-A.

The above described method is called forward spatial smoothing. Another proposed method ([11]) that is more effective is forward backward spatial smoothing. The method is presented below.

For forward backward spatial smoothing, the array is also divided into subarrays in backward direction (See Figure 15).

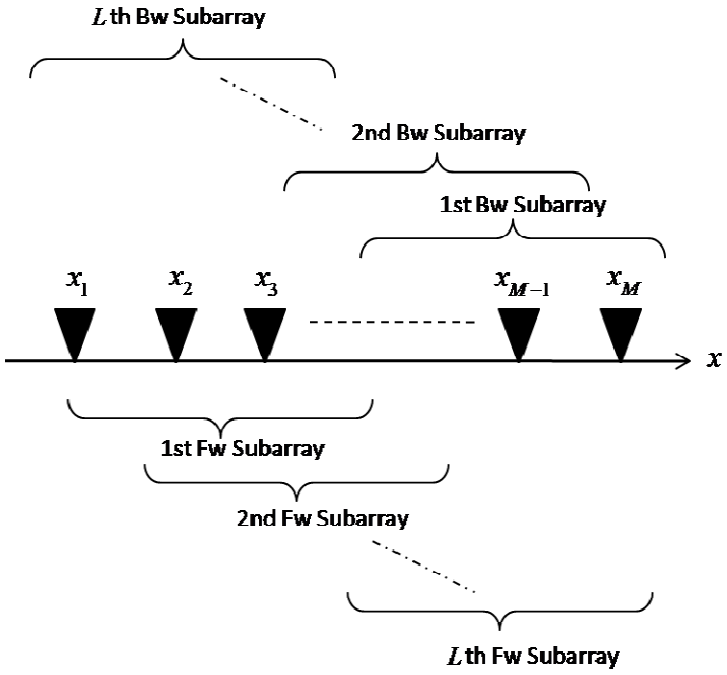

Figure 15 Division of an M-element ULA into Subarrays for Forward Backward Spatial Smoothing

The MxM permutation matrix is defined as

$$Q = \begin{pmatrix} 0 & 0 & \cdots & 1 \\ \vdots & \vdots & \iddots & \vdots \\ 0 & 1 & \cdots & 0 \\ 1 & 0 & \cdots & 0 \end{pmatrix} \tag{3.41}$$

The received signal by the l th backward subarray can be expressed as

$$r_l^b(t) = Qr_l^*(t) = QA^*D_l^*S^*(t) + Qn_l^*(t) \tag{3.42}$$

Below given equation is valid for uniform linear arrays

$$QA^*D_l^* = AD_l^{(b)} \tag{3.43}$$

where $D_l^{(b)}$ is an NxN diagonal matrix.

$$D_l^{(b)} = diag\{e^{-j\pi d(M_0+l-2)\sin\theta_1},\ldots,e^{-j\pi d(M_0+l-2)\sin\theta_N}\} \tag{3.44}$$

The autocorrelation matrix of the received signal by the l th backward subarray can be denoted as follows:

$$R_l^{(b)} = AD_l^{(b)}R_s^*(D_l^{(b)})^H A^H + \sigma^2 I \tag{3.45}$$

The backward spatially smoothed autocorrelation matrix is the average of the subarrays' autocorrelation matrices

$$\overline{R}^{(b)} = \frac{1}{L}\sum_{l=1}^{L} R_l^{(b)} \tag{3.46}$$

By putting (3.45) into (3.46) below given expression is obtained.

$$\overline{R}^{(b)} = A(\frac{1}{L}\sum_{l=1}^{L} D_l^{(b)}R_s^*(D_l^{(b)})^H)A^H + \sigma^2 I \tag{3.47}$$

After simplifying (3.47) backward smoothed autocorrelation matrix can be written as

$$\overline{R}^{(b)} = A\overline{R_s}^{(b)}A^H + \sigma^2 I \tag{3.48}$$

where $\overline{R_s}^{(b)}$ is defined as

$$\overline{R_s}^{(b)} = \frac{1}{L}\sum_{l=1}^{L} D_l^{(b)}R_s^*(D_l^{(b)})^H \tag{3.49}$$

Then by combining (3.48) and (3.39), forward backward smoothed autocorrelation matrix can be obtained as

$$\overline{R}^{(fb)} = \frac{1}{2}(\overline{R}+\overline{R}^{(b)}) = \frac{1}{2}A(\overline{R_s}+\overline{R_s}^{(b)})A^H + \sigma^2 I \tag{3.50}$$

In [11], it is shown that, each subarray can be used twice: once in computing the forward smoothed autocorrelation, and once in computing the backward smoothed autocorrelation. Thus, to resolve N signals independent of their coherency, $N/2$ subarrays of length $M_0 = M+1-N/2$ are sufficient. However, for forward only smoothing, number of required subarrays is N, and the subarray size decreases in this case to $M_0 = M+1-N$. This means that as compared to forward only spatial

smoothing, forward backward spatial smoothing uses the same number of array sensors more effectively.

In [14], Friedlander demonstrated that above described spatial smoothing schemes are not just limited to ULA. Any array which can be subdivided into subarrays which all have the same configuration, but are shifted with respect to each other, is suitable to perform forward spatial smoothing. For example, a square array with size $M_1 x M_1$, can be divided into square subarrays with size $M_2 x M_2$ each. The steering vector of a subarray shifted by $(\Delta x, \Delta y)$ with respect to the reference subarray, A_s , is related to the steering vector of a reference subarray, A_r , as follows:

$$A_s = A_r D_s = A_r diag\left\{e^{j\pi(\Delta x \sin\theta_1 + \Delta y \cos\theta_1)}, \ldots, e^{j\pi(\Delta x \sin\theta_N + \Delta y \cos\theta_N)}\right\} \tag{3.51}$$

Using this relationship, forward smoothing technique can be applied. For the backward smoothing, the condition is more restrictive, such that each array must have center symmetry as defined by: $x_m - x_1 = x_M - x_{M-m+1}$ and $y_m - y_1 = y_M - y_{M-m+1}$, for $m = 1, \ldots, M$, where (x_m, y_m) are the coordinates of the m th sensor of the subarray.

The above given requirements on array geometries restrict the application of spatial smoothing. Therefore, in [14] interpolation technique is proposed to perform these methods by using arbitrary array geometries. Interpolation technique is presented in the next section.

3.5 INTERPOLATION

Array interpolation is a method that allows a mapping from the real array structure to a desired virtual array. It is first introduced by Friedlander in [23] to extend the Root MUSIC algorithm which is restricted to ULA to arbitrary array geometries and afterwards used to address the different issues related to direction finding as coherent signals problem and direction finding of wideband signals ([14], [24]).

Outputs of the virtual array can be obtained by a linear interpolation technique, with the interpolator coefficients selected so as to minimize the interpolation error for signals arriving from a given sector. Different sets of interpolator coefficients will be

used to provide good estimates for different sectors. The design of the interpolator needs to be performed only once, and can be done off-line.

In most cases calculating the output of virtual array is not required since the autocorrelation matrix will be enough to apply direction finding methods. In the below given steps the way of finding the autocorrelation matrix, the signal and noise subspace of an interpolated array based on the autocorrelation matrix of the real array is explained.

1. Divide the field of view of the array into sectors. The k th sector is defined by the interval $\left[\theta_k^{(1)}, \theta_k^{(2)}\right]$ where $\theta_k^{(1)}$ and $\theta_k^{(2)}$ are start and end angles of the sector.

2. Select a step size $\Delta\theta$ and define the set of angles

$$\Theta_k = \left[\theta_k^{(1)}, \theta_k^{(1)} + \Delta\theta, \theta_k^{(1)} + 2\Delta\theta, \cdots, \theta_k^{(2)}\right] \tag{3.52}$$

   assuming that $\theta_k^{(2)} - \theta_k^{(1)}$ is an integer multiple of $\Delta\theta$.

   These angles are only used in the design of interpolation coefficient.

3. Compute the array manifold of the real array, A_k, for the set of angles Θ_k.

$$A_k = \left[a(\theta_k^{(1)}), \cdots, a(\theta_k^{(2)})\right] \tag{3.53}$$

   Note that A_k is a section of the array manifold of the real array.

4. Decide the desired locations of the virtual elements of the interpolated array and compute the array manifold of the interpolated array, $\overline{A_k}$, for the same set of angles Θ_k.

$$\overline{A_k} = \left[\overline{a}(\theta_k^{(1)}), \cdots, \overline{a}(\theta_k^{(2)})\right] \tag{3.54}$$

   In other words, A_k is the response of the real array to signals arriving from directions Θ_k, and $\overline{A_k}$ is the response of the interpolated array to the signals arriving from same directions.

5. It is possible to obtain the array manifold of the interpolated array by linear interpolation of the array manifold of the real array within each sector k. This means that there exists a coefficient matrix B_k such that

$$B_k A_k = \overline{A_k} \tag{3.55}$$

For sure, the above interpolation is an approximation, therefore the equation does not really hold. The best fit between the interpolated response $B_k A_k$ and the desired response $\overline{A_k}$ should be found to obtain the best interpolation matrix. This means, the interpolation coefficient is computed as the least squares solution of (3.55).

$$B_k = \overline{A_k} A_k^H (A_k A_k^H)^{-1} \tag{3.56}$$

6. The autocorrelation matrix of the interpolated array can be obtained by using the interpolation coefficient and by using the autocorrelation matrix of the real array as follows:

$$\overline{R_k} = B_k R B_k^H \tag{3.57}$$

7. It is also possible to compute directly the signal subspace of the interpolated array without computing the autocorrelation matrix of it. Let E_s be the signal subspace that belongs to the real array and $\overline{E_s}$ denote the signal subspace of the interpolated array. Then the relation between E_s and $\overline{E_s}$ is

$$\overline{E_s} = B_k E_s \tag{3.58}$$

8. The noise subspace $\overline{E_n}$ of the interpolated array can be found by calculating the subspace orthogonal to $\overline{E_s}$. This can be done by QR decomposition method [23]. After QR decomposition of the MxN matrix $\overline{E_s}$, last $M - N$ columns of Q will give $\overline{E_n}$.

9. When calculating the polynomial in Root MUSIC method mentioned in Section 3.2, the interpolated noise subspace $\overline{E_n}$ obtained in step 8 can be used.

3.6 CONVENTIONAL ROOT MUSIC WITH SPATIAL SMOOTHING AND INTERPOLATON

After examining the spatial smoothing and interpolation methods in previous sections, in this section the Conventional Root MUSIC technique will be combined with these methods.

In Section 3.4, it was stated that spatial smoothing is limited to special array geometries. If the array geometry is random or is not suitable for direct implementation of spatial smoothing (e.g., Uniform Circular Array), then interpolation can be applied to convert the real array to a virtual array that is appropriate for spatial smoothing.

In [14], three different methods are described and compared as depicted in Figure 16. These methods are distinguished by their interpolated array configurations. In the

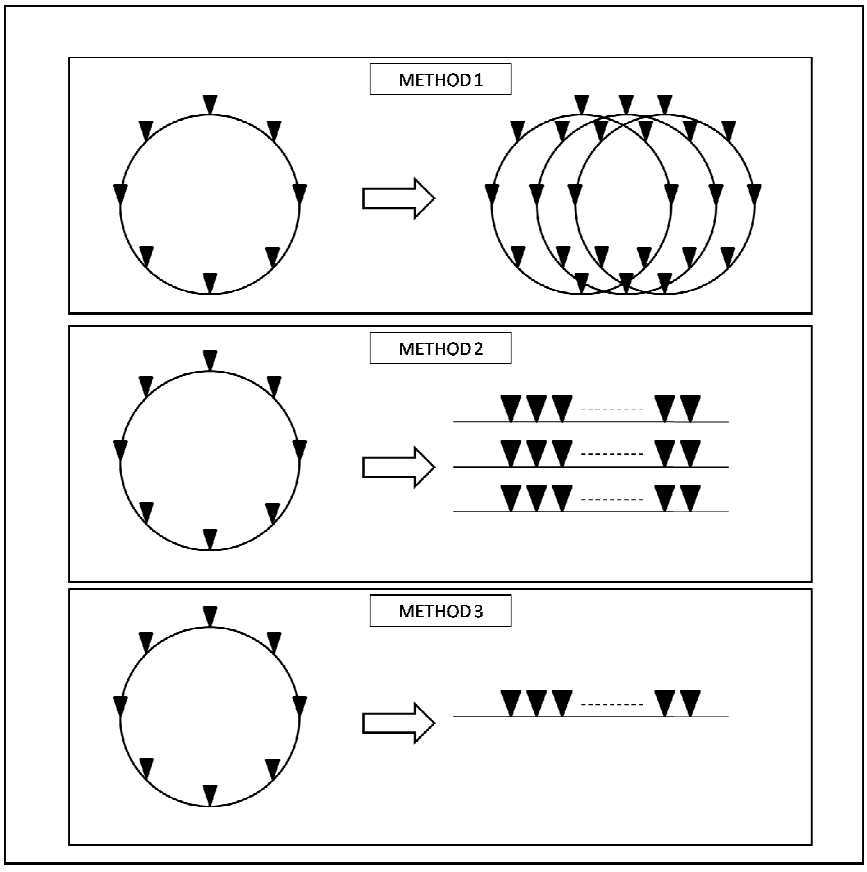

Figure 16 Alternative Interpolation Methods

first method interpolated arrays are shifted versions of real array with the same shape. Then these shifted versions of real arrays are used as subarrays while performing spatial smoothing. In this method since the formed subarrays do not generate a Vandermonde array manifold structure, DOAs can be found by Spectral MUSIC algorithm instead of Root MUSIC that is faster. Second suggested method permits the usage of Root MUSIC because the generated interpolated arrays are uniform linear arrays, and therefore, faster. In this method real array is interpolated into multiple linear arrays all having the same number of elements as the original array where each is a shifted version of other. Third and the last method proposes to create only one linear interpolated array and to divide this into overlapping subarrays that can be used for spatial smoothing process. Among these methods, the last one is introduced as the most effective one.

In this thesis, the real array structure is assumed as a Uniform Circular Array and the third method is preferred to convert the manifold of the real array to the manifold of a Uniform Linear Array form. This interpolated Uniform Linear Array has the same aperture and the same number of elements as the original array. Real array and interpolated array structures are shown in Figure 17 .

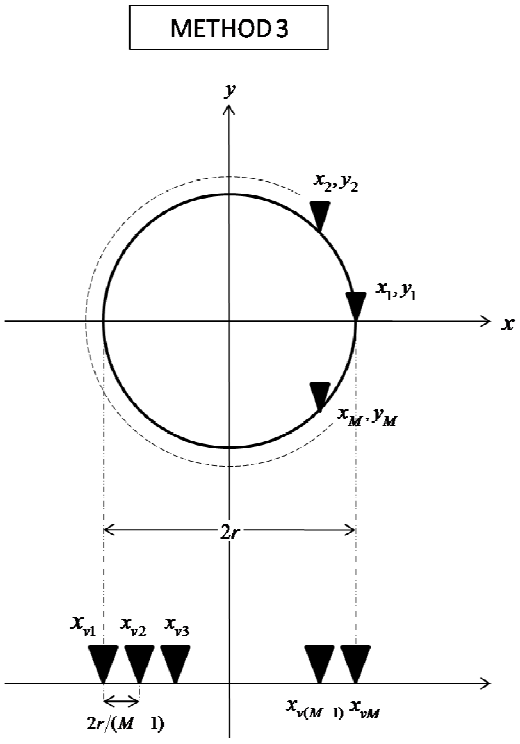

Figure 17 Preferred Interpolation Method

The application of the Conventional Root MUSIC with forward backward spatial smoothing and interpolation can be summarized as follows:

1. Select the start and end angles of sector; $\left[\theta_k^{(1)}, \theta_k^{(2)}\right]$.

2. Compute the interpolation coefficient, B_k, for the selected sector. (Note that for a given array, it is enough to calculate B_k only once and offline.)

   a. Array manifold of the real array, A_k, can be written by using the below given steering vector

$$a(\theta) = \begin{pmatrix} e^{j\pi(x_1 \sin\theta + y_1 \cos\theta)} \\ \vdots \\ \vdots \\ e^{j\pi(x_M \sin\theta + y_M \cos\theta)} \end{pmatrix} \tag{3.59}$$

   where

$$x_m = r.\cos\left(\frac{2\pi(m-1)}{M}\right) \tag{3.60}$$

$$y_m = r.\sin\left(\frac{2\pi(m-1)}{M}\right) \tag{3.61}$$

   for $m = 1, \ldots, M$.

   b. Array manifold of the interpolated array, $\overline{A_k}$, can be written by using the below given steering vector

$$\overline{a}(\theta) = \begin{pmatrix} e^{j\pi(x_{v1} \sin\theta)} \\ \vdots \\ \vdots \\ e^{j\pi(x_{vM} \sin\theta)} \end{pmatrix} \tag{3.62}$$

   where

$$x_{vm} = \frac{2r}{M-1}\left\{(m-1) - \left(\frac{M-1}{2}\right)\right\} \tag{3.63}$$

   for $m = 1, \ldots, M$ and where the origin of the array is assumed to be the center point of the ULA.

c. Then B_k can be computed by using (3.55) and (3.56).

3. Estimate the autocorrelation matrix of the real array by using the set of snapshots of the received signal.

$$\hat{R} = \frac{1}{T_{obs}} \sum_{t=1}^{T_{obs}} r(t) r(t)^H \tag{3.64}$$

4. Calculate the autocorrelation matrix of the interpolated array with the B_k found in step 2.c.

$$\hat{\bar{R}} = B_k \hat{R} B_k^H \tag{3.65}$$

5. Construct the matrix

$$R_1 = \hat{\bar{R}} + Q \hat{\bar{R}}^* Q \tag{3.66}$$

where Q is an MxM permutation matrix.

6. Forward backward spatially smoothed autocorrelation matrix is expressed as below:

$$R^{(fb)} = \frac{1}{2L} \sum_{l=1}^{L} Z_l^T R_1 Z_l \tag{3.67}$$

where Z_l consists of M_0 columns of the MxM identity matrix as follows:

$$Z_l = [e_l, e_{l+1}, \ldots, e_{l+M_0-1}] \tag{3.68}$$

Then, $R^{(fb)}$ will be nonsingular again if the number of subarrays, L, is selected appropriately. For the worst case, i.e., all the signals are coherent, to obtain a nonsingular autocorrelation matrix after spatial smoothing the number of the impinging signals, L should be selected as greater than the number of incoming signals N.

7. Perform the same procedure on the noise correlation matrix;

a. If the noise is assumed to be uncorrelated from sensor to sensor and to have variance σ^2, then noise autocorrelation matrix is diagonal.

$$R_n = \sigma^2 I \tag{3.69}$$

b. Obtain the autocorrelation matrix of the noise output of the interpolated array

$$\overline{R_n} = \sigma^2 B_k B_k^H \tag{3.70}$$

c. Perform spatial smoothing operation for $\overline{R_n}$.

$$R_n^{(fb)} = \frac{1}{2L}\sum_{l=1}^{L} Z_l^T(\overline{R_n} + Q\overline{R_n}^* Q)Z_l \tag{3.71}$$

8. Noise autocorrelation matrix that is found in step 7.b. has colored structure after interpolation since its diagonal form is disturbed. Therefore whitening of $R^{(fb)}$ is required.

$$\widehat{R} = \left[R_n^{(fb)}\right]^{-1/2} R^{(fb)} \left[R_n^{(fb)}\right]^{-H/2} \tag{3.72}$$

9. Perform EVD for $\widehat{R}$ and find noise subspace, $\widehat{E_n}$, by using the eigenvectors corresponding to the minimal $M-N$ eigenvalues.

10. DOAs can be found by solving the following equation. Note that the equation in (3.19) should be modified to reflect the effect of whitening [14].

$$\left\| \overline{a}(\theta)^H \left[R_n^{(fb)}\right]^{-1/2} \widehat{E_n} \right\| = 0 \tag{3.73}$$

a. $\overline{a}(\theta)$ is the steering vector of one of the subarrays of the interpolated array.

$$\overline{a}(\theta) = e^{j\pi\frac{2r}{M-1}\sin\theta[-\frac{M-1}{2} \quad 1-\frac{M-1}{2} \quad \cdots \quad (M_0-1)-\frac{M-1}{2}]^T} \tag{3.74}$$

b. Rewriting in $e^{-j\pi(\frac{M-1}{2})(\frac{2r}{M-1})\sin\theta}$ parenthesis

$$\overline{a}(\theta) = e^{-j\pi(\frac{M-1}{2})(\frac{2r}{M-1})\sin\theta}\left[1 \quad e^{j\pi\frac{2r}{M-1}\sin\theta} \quad \cdots \quad e^{j(M_0-1)\pi\frac{2r}{M-1}\sin\theta}\right] \tag{3.75}$$

c. Say $\phi = \pi(\dfrac{2r}{M-1})\sin\theta$

$$\overline{a}(\phi) = e^{-j(\frac{M-1}{2})\phi}[1 \quad e^{j\phi} \quad \cdots \quad e^{j(M_0-1)\phi}] \tag{3.76}$$

d. Then the steering vector can be written in terms of $z = e^{j\phi}$ as follows:

$$\bar{a}(z) = z^{-\frac{M-1}{2}}[1 \quad z \quad \cdots \quad z^{M_0-1}]^T \tag{3.77}$$

e. (3.73) can be expressed as a polynomial with degree $2(M_0 - 1)$.

f. This polynomial has $2(M_0 - 1)$ roots and these roots will give us the candidates for solution of z. Correct roots can be selected as described in Section 3.2.

g. After selecting the correct roots, the estimates of the DOAs for N impinging signals can be found by using the following equations:

$$\phi = \arg(z) \tag{3.78}$$

$$\theta = \arcsin(\frac{\phi(M-1)}{2\pi r}) \tag{3.79}$$

3.7 CYCLIC ROOT MUSIC WITH SPATIAL SMOOTHING AND INTERPOLATON

In this section, Cyclic Root MUSIC technique will be combined with forward backward spatial smoothing and interpolation methods. Same real and interpolated array configurations are considered as in Section 3.6 (Figure 17). The implementation can be summarized as follows:

1. Repeat the steps 1 and 2 of Section 3.6 to compute the interpolation coefficient, B_k, of the selected sector.

2. Estimate the cycle frequency α and the time lag τ parameters for the SOIs whose DOAs are desired to be found as described in Chapter 2.

3. Estimate the cyclic autocorrelation matrix of the real array by using the set of snapshots of the received signal.

$$\widehat{R^{\alpha}}(\tau) = (1/T_{obs})\sum_{t=1}^{T_{obs}} r(t+\tau/2)r^H(t-\tau/2)e^{-j2\pi\alpha t} \tag{3.80}$$

4. Find the cyclic autocorrelation matrix of the interpolated array for the selected sector

$$\overline{R_k^{\alpha}}(\tau) = B_k \widehat{R^{\alpha}}(\tau) B_k^H \tag{3.81}$$

5. Construct the matrix

$$R_1^{\alpha}(\tau) = \overline{R_k^{\alpha}}(\tau) + Q\overline{R_k^{\alpha}}(\tau)^* Q \tag{3.82}$$

where Q is an MxM permutation matrix.

6. Forward backward spatially smoothed autocorrelation matrix is calculated as follows:

$$\widehat{R^{\alpha}}(\tau)^{(fb)} = \frac{1}{2L}\sum_{l=1}^{L} Z_l^T R_1^{\alpha}(\tau) Z \tag{3.83}$$

where Z_l consists of M_0 columns of the MxM identity matrix

$$Z_l = [e_l, e_{l+1}, \ldots, e_{l+M_0-1}] \tag{3.84}$$

After applying spatial smoothing, $\widehat{R^{\alpha}}(\tau)^{(fb)}$ will be nonsingular again with suitable selection of subarray number. If all SOIs sharing the same cycle frequency are fully correlated, subarray number, L, should be selected greater than the number of incoming SOIs to obtain a cyclic autocorrelation function of rank K.

Note that for Cyclic Root MUSIC method no whitening operation is required as in Conventional Root MUSIC since the effect of noise component is effectively eliminated from the cyclic autocorrelation matrix.

7. Perform EVD for $\widehat{R^{\alpha}}(\tau)^{(fb)}$ and find the noise subspace, $\widehat{E_n}$, corresponding to the minimal ($M - K$) eigenvalues.

8. Then similar operation in step 10 of Section 3.6 should be carried out to estimate the DOA's. However, instead of selecting N roots closest to unit circle as in Conventional Root MUSIC, K roots should be selected since the aim is just to find the DOAs of SOIs.

CHAPTER 4

SIMULATIONS

In this section, behaviors of the Conventional Root MUSIC and Cyclic Root MUSIC in the existence of coherency between the SOIs are compared by simulation results. It is considered that signals are received by a UCA. Therefore interpolation method is used in conjunction with spatial smoothing.

Here a uniformly spaced circular array with $M = 8$ sensors with radius r is considered. This UCA is interpolated to a ULA whose total aperture is equal to the diameter of the UCA. Total number of sensors in ULA is assumed to be the same as the number of sensors in UCA. Therefore, distance between the adjacent sensors of the interpolated array is $2r/(M-1)$. To avoid ambiguity, spacing between the adjacent sensors of the ULA should be at most $\lambda/2$.

$$d(ULA) = 2r/(M-1) = \lambda/2 \tag{4.1}$$

The relation between the radius of the UCA and the distance between the adjacent sensors of the UCA can be expressed as follows (See Figure 18):

$$\frac{d(UCA)}{2} = r\sin(\frac{\pi}{M}) \tag{4.2}$$

$$r = d(UCA)\Big/ 2\sin\frac{\pi}{M} \tag{4.3}$$

By combining (4.1) and (4.3), the required spacing between the adjacent sensors of the UCA to avoid ambiguity can be found as $2.67\,\lambda/2$.

Four different signal scenarios are considered in simulations.

- Two coherent BPSK modulated SOIs using the same bit rate,

- Two coherent BPSK modulated SOIs using the same bit rate and one BPSK modulated SNOI whose bit rate is multiple of the SOIs' bit rate,
- Two coherent BPSK modulated SOIs using the same bit rate and one BPSK modulated SNOI whose bit rate is not multiple of the SOIs' bit rate,
- Two coherent BPSK modulated SOIs using the same bit rate and one Amplitude Modulated SNOI.

In these scenarios SOIs are assumed to be fully correlated, BPSK modulated, cyclostationary signals with 4 Mb/s bit rate. In the second and third scenarios the bit rate of SNOI is considered to be 8 Mb/s and 3.2 Mb/s, respectively. Last scenario includes an Amplitude Modulated SNOI with 50% modulation depth.

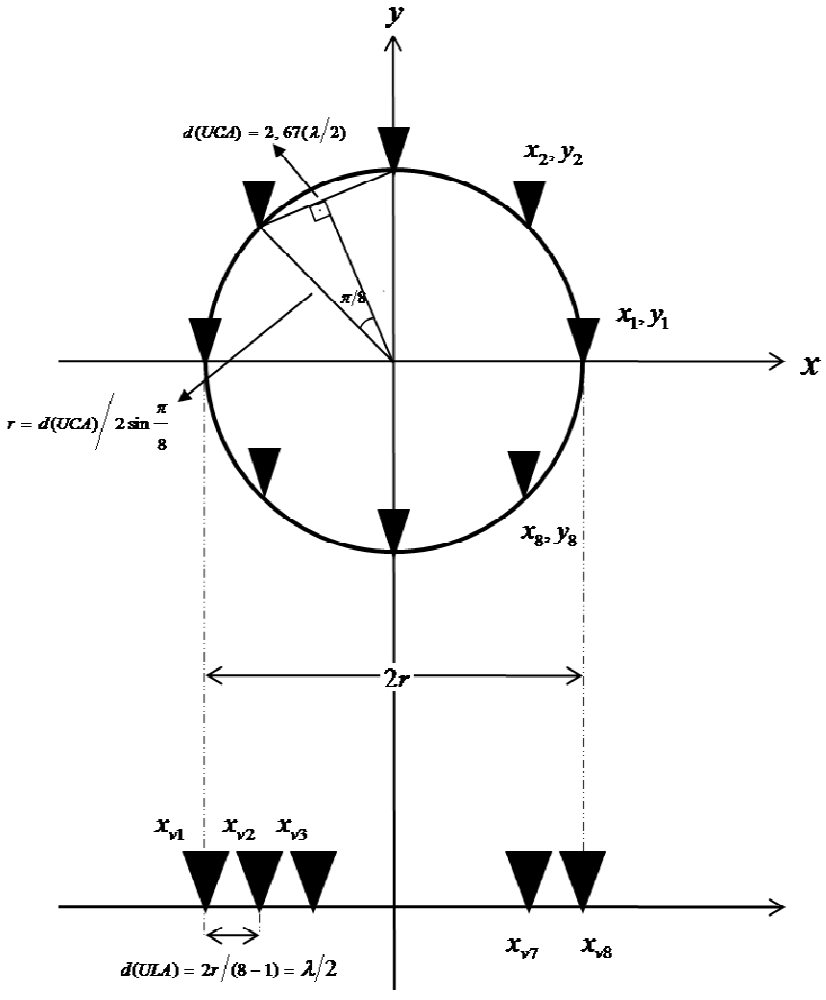

Figure 18 Real and Interpolated Array Structure Used in Simulations

BPSK signals can be expressed as follows:

$$s(t) = A\sin(2\pi f_c t + \psi) \tag{4.4}$$

where A is the amplitude, f_c is the carrier frequency, and ψ is the varying phase of a BPSK signal.

AM signals can be expressed as follows:

$$s(t) = \left[A + M\cos(2\pi f_m t)\right]\sin(2\pi f_c t) \tag{4.5}$$

where f_m is the center frequency and M is the peak value of the message to be transmitted.

The carrier frequency of the incoming signals, f_c, is assumed to be 10 MHz. Sampling frequency is 32 MHz.

The phase of the BPSK signals is generated randomly, i.e., either 0 or π with probability $1/2$. An example of generating the BPSK signals is illustrated in Figure 19. Here total observation duration, T_{obs}, is considered as 100 μs. For a BPSK signal whose bit rate is equal to 4 Mb/s, the phase (ψ) may change between 0 and π in every $1/4x10^6$ seconds. If this BPSK signal is sampled with a sample rate $1/32x10^6$ seconds, the same data will be received in the adjacent $K = 8$ snapshots since the phase of the signal stays unchanged in a symbol. From the ratio between total observation duration ($T_{obs} = 100$ μs) and bit rate ($T = 1/4x10^6$ s), it can be found that total number of the symbols during the observation time is $L = 400$. This means $KxL = 3200$ snapshots should be generated for 100 μs observation duration.

After obtaining BPSK signal samples as explained in the above paragraph, coherency condition between the SOIs should be generated. Firstly, two uncorrelated BPSK signals $\underline{s}_1(t)$ and $\underline{s}_2(t)$ are constructed. Then, incoming coherent SOIs, $s_1(t)$ and $s_2(t)$, are generated as follows:

$$s_1(t) = \underline{s}_1(t) \tag{4.6}$$

$$s_2(t) = \rho\underline{s}_1(t) + \sqrt{1-\rho^2}\,\underline{s}_2(t) \tag{4.7}$$

where ρ is the correlation coefficient that is described as in [14]. This means;

- $\rho = 1 \rightarrow$ SOIs are *fully correlated* (*coherent*),
- $\rho = 0 \rightarrow$ SOIs are *uncorrelated*,
- $0 < \rho < 1 \rightarrow$ SOIs are *partially correlated*.

$\rho = 1$ is used in simulations.

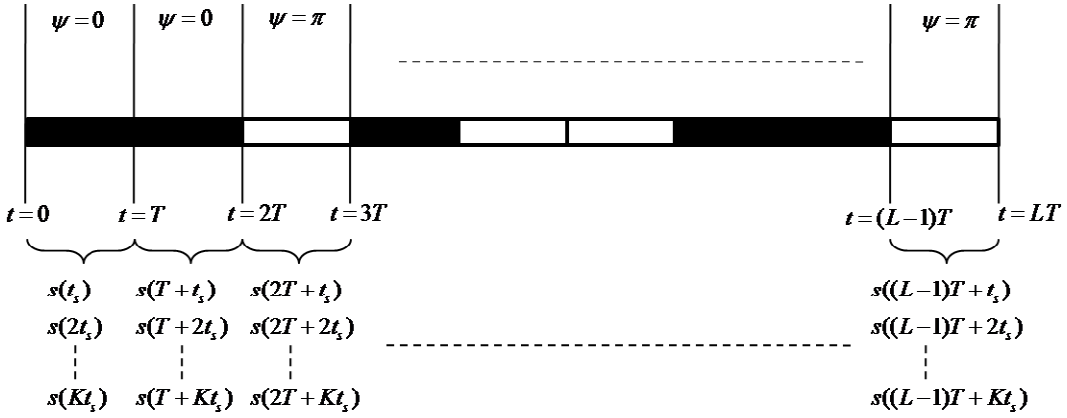

$$s(t) = \begin{cases} A\sin(2\pi f_c t) \text{ where } \psi = 0 \\ A\sin(2\pi f_c t + \pi) \text{ where } \psi = \pi \end{cases}$$

$$\left.\begin{array}{l} T = \dfrac{1}{4x10^6} = 0.25\mu s \\ t_s = \dfrac{1}{32x10^6} = 0.03125\mu s \\ T_{obs} = 100\mu s \end{array}\right\} \quad \begin{array}{l} K = \dfrac{T}{t_s} = 8 \\ L = \dfrac{T_{obs}}{T} = 400 \end{array}$$

Figure 19 BPSK Signal with given Bit Rate, Sampling Frequency, and Observation Time

To overcome the coherency problem, in simulations the spatial smoothing technique is performed with 2 forward subarrays and 2 backward subarrays of length 7 each. This degree of spatial smoothing is sufficient for the used signal scenario, i.e., two coherent signals. In [25], it is emphasized that performing a high degree of spatial smoothing by dividing the array into subarrays more than required, will cause a decrease on the performance of the spatial smoothing algorithm.

To apply cyclostationary based algorithms for the above given BPSK signal cycle frequency and lag parameters should be estimated. For this purpose magnitude of the cyclic autocorrelation function for a 4 Mb/s BPSK modulated signal with respect to variable cycle frequency and lag parameters can be calculated. As explained in Chapter 2, for a 4 Mb/s BPSK modulated signal $\alpha = 4MHz$ and $\tau = 0.125\mu s$ (See Figure 4 and Figure 5).

The statistical reliability of the simulations is obtained by independent experiments. In the simulations, the results of 50 independent experiments are used to compute the estimated RMS error and the bias for each DOA estimate.

To define SNR value in the simulations, signal power is kept as constant and noise power is scaled according to SNR value. Signal power is assumed as the power of one of the signals if all the signals have equal power or is assumed as the power of the strongest signal if all the signals do not have equal power. By this way the weaker signals are more exposed to noise compared to the stronger ones.

In calculating the RMS error for DOA estimations, the following criterion is used to remove the effects of gross errors: If more than 10% of the experiments yield gross errors, then the algorithm is assumed to be useless (not working). If 10% or less of experiments yield gross errors, then the experiment results with gross errors are eliminated (not included in RMSE calculation). The DOA estimates which deviate 5^o from the real DOA are considered as "gross errors". Unless otherwise stated, it must be understood that all the results of all independent experiments are used for the statistics.

Throughout this chapter, if the behavior of RMSE graphs for SOI1 and SOI2 are similar, only the graph for SOI2 is illustrated since SNOI is always located at a closer angle to SOI2 than SOI1. If the behavior of RMSE graphs for SOI1 and SOI2 are different, both of the graphs are depicted.

Cramér-Rao Bound (CRB) calculations for RMSE are also included into the graphs. To calculate the CRB, close form expression which is derived in [27] and [28] is used. For completeness, this close form expression is also included in Appendix-B.

Simulations are carried out for various effects. Performance of Cyclic Root MUSIC and Conventional Root MUSIC are compared under the variation of the following factors; interpolation sector, SNR, spatial separation between SOIs or between SOIs and SNOI, total observation duration, power difference between SOIs or between SOIs and SNOI. These influences are investigated for different signal scenarios. Throughout the simulations, performance of Cyclic Root MUSIC is compared for three signal scenarios which differ in SNOI types. Comparison of Conventional Root MUSIC under different SNOI types is not considered since Conventional Root MUSIC is not affected from the cyclostationarity properties of the signals.

4.1 EFFECT OF INTERPOLATION SECTOR

In this section, simulation results are illustrated to observe the effect of interpolation sector on the performances of Cyclic Root MUSIC and Conventional Root MUSIC algorithms.

Total observation duration is considered as 100 μs. DOAs of SOI1 and SOI2 are kept constant as 5^o and 30^o, respectively. Two different interpolation sectors are compared; 0^o-45^o and 0^o-65^o. For both of the interpolation sectors, the same step size, 0.01, is used. It is considered that no SNOI exists in the environment.

In Figure 20, variation of RMSE for SOI2 under varying SNR is given. Figure 20 compares two different interpolation sectors; 0^o-45^o and 0^o-65^o when no SNOI exists. From this figure, it can be seen that performance of the narrower sector is better for both DOA estimation methods.

Figure 21 and Figure 22 show the biases of Conventional Root MUSIC and Cyclic Root MUSIC at SNR=15 dB when no SNOI exists, respectively. As can be seen from these figures, wider interpolation sector causes a considerable increase on the bias for Conventional Root MUSIC although the bias stays almost similar for Cyclic Root MUSIC. It is observed that this bias of Conventional Root MUSIC exists for all SNR values. Therefore, in Figure 20, a flat RMSE characteristic is obtained for Conventional Root MUSIC when 0^o-65^o interpolation sector is selected.

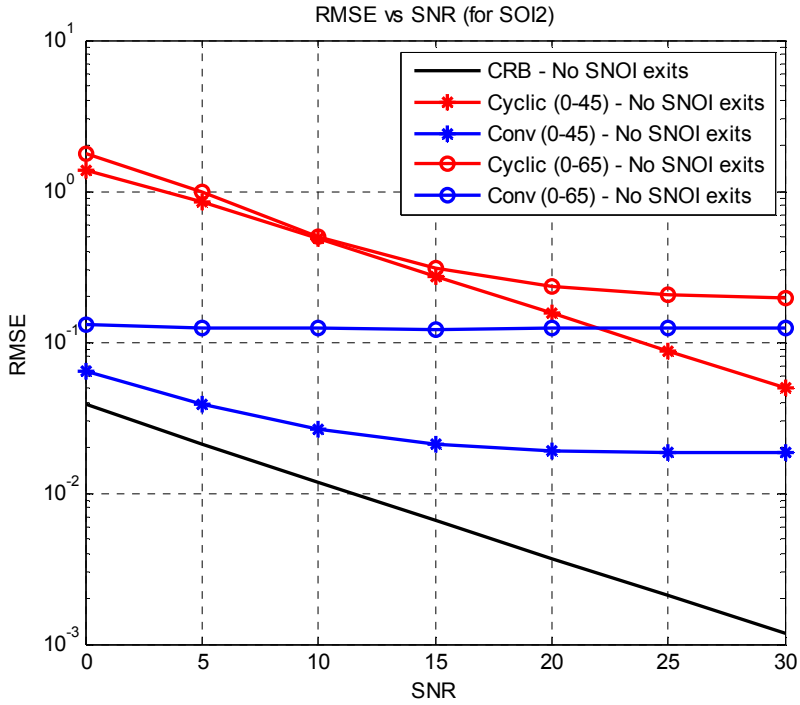

Figure 20 Variation of RMS error for SOI2 as a function of SNR when DOA of SOI1 is 5°, DOA of SOI2 is 30°. Two different interpolation sectors are compared; 0°-45° and 0°-65° (No SNOI exist)

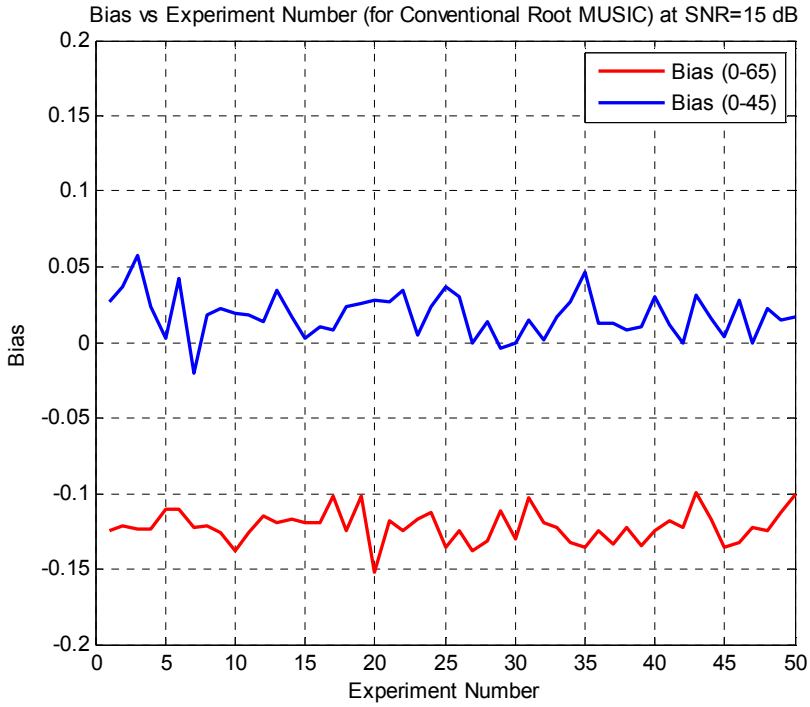

Figure 21 Bias of the estimated DOAs of SOI2 by Conventional Root MUSIC at SNR=15dB. Two different interpolation sectors are compared; 0°-45° and 0°-65° (No SNOI exist)

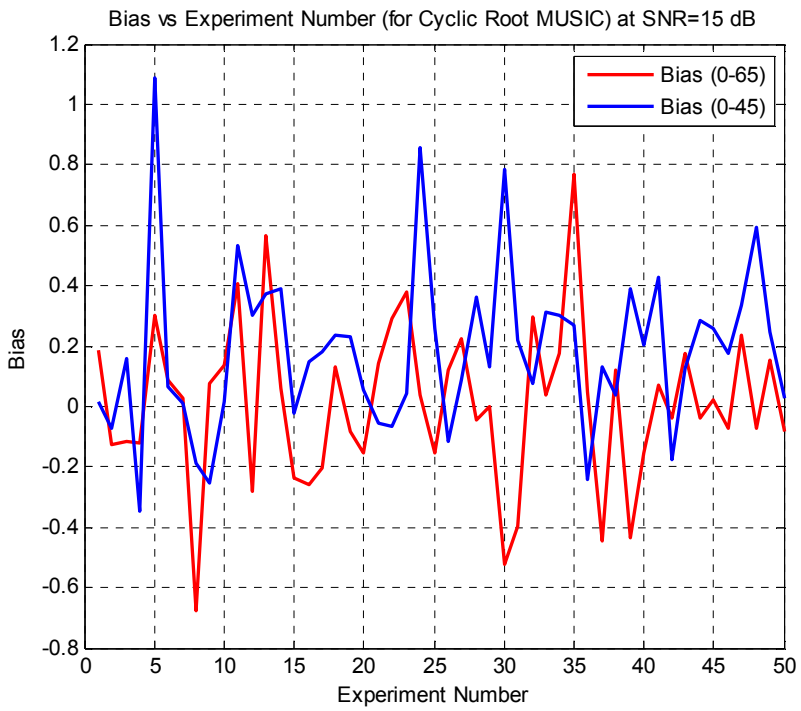

Figure 22 Bias of the estimated DOAs of SOI2 by Cyclic Root MUSIC at SNR=15dB. Two different interpolation sectors are compared; 0^o-45^o and 0^o-65^o (No SNOI exist)

Necessity of selecting narrower sectors was also explained in [23]. It was recommended to design the array so that $\left\|\overline{A_k} - B_k A_k\right\|_F \Big/ \left\|\overline{A_k}\right\|_F$ to be on the order of 10^{-3} or smaller where $\overline{A_k}$, A_k, B_k are defined in Section 3.5 and where $\|.\|_F$ denotes the Frobenius norm. This ratio between the error norm and the array manifold norm is equal to 0.0031 for 0^o-45^o interpolation sector. The ratio increases to 0.0284 for 0^o-65^o interpolation sector.

In [23] , interpolation method was inspected only for Conventional Root MUSIC and it was stated that required criterion for the ratio between the error norm and the array manifold norm was obtained experimentally. In this work, it is observed that Cyclic Root MUSIC shows more robust behavior against sector changes. However, narrower sector is still better for Cyclic Root MUSIC, too.

As a result, it is observed that 0^o-45^o interpolation sector with 0.01 step size is more suitable for both methods. Therefore, these values are used for the remaining simulations of the chapter.

4.2 EFFECT OF SNR

In this section, performance of Cyclic Root MUSIC and Conventional Root MUSIC are compared under increasing SNR value.

In the following, the results of simulations that show the effect of varying SNR are presented and discussed while keeping the total observation duration, DOA separation of SOIs and interpolation sector constant. Total observation duration is considered as 100 μs. SOI1 arrives to the array from 5^o, SOI2 arrives to the array from 30^o. Interpolation sector is selected as 0^o-45^o with 0.01 step size.

Figure 23 shows the variation of RMSE for SOI2 as a function of SNR when no SNOI exists. As can be seen from this figure, by the use of Conventional Root MUSIC, less RMSE values are obtained than that of the Cyclic Root MUSIC. It can be seen that although Cyclic Root MUSIC is known as an algorithm which eliminates the background noise, it is also affected from the increase of SNR value. Certainly noise does not show cyclostationarity properties, but under high noise powers cyclostationarity characteristic of the SOI will also be deteriorated.

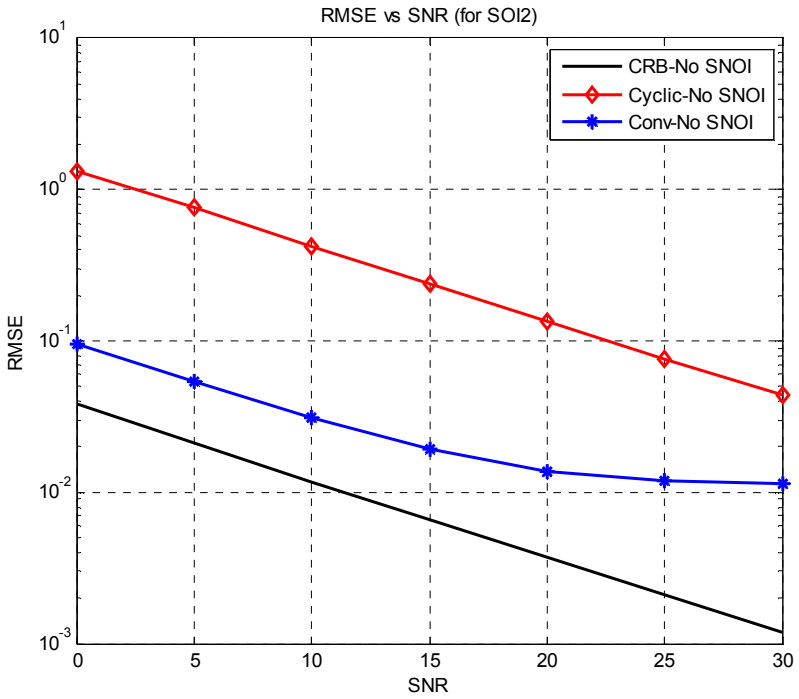

Figure 23 Variation of RMS error for SOI2 as a function of SNR when the DOA of SOI1 is 5^o, DOA of SOI2 is 30^o (No SNOI exists)

Figure 24-Figure 26 compare the Cyclic Root MUSIC and Conventional Root MUSIC algorithms in the existence of a SNOI at 35° for three different SNOI types. These figures show that Conventional Root MUSIC has better performance than Cyclic Root MUSIC even in the existence of a SNOI when SNOI is sufficiently separated from SOI2. From the comparison of the figures, it can be seen that Cyclic Root MUSIC has the best results when the SNOI is an AM signal. For BPSK modulated signals, Cyclic Root MUSIC provides better results if the bit rate of the SNOI is not a multiple of bit rate of SOI. When the bit rate of the SNOI is a multiple of bit rate of SOI, this causes to obtain non zero cyclic autocorrelation values for SNOI by using the cycle frequency of SOI (See Figure 8 and Figure 9 in Chapter 2). This means, SNOI cannot be isolated properly in multiple bit rate case in Cyclic Root MUSIC application.

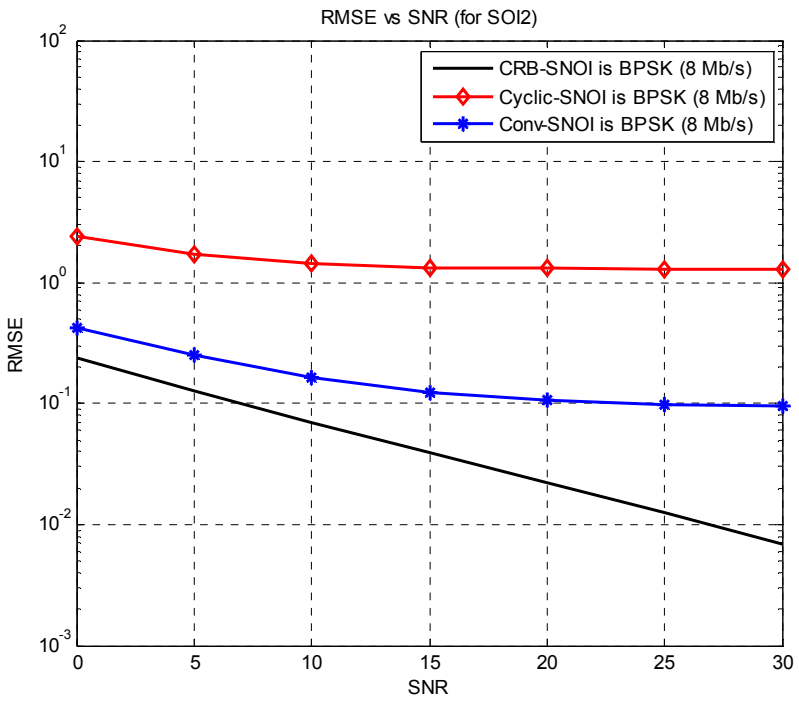

Figure 24 Variation of RMS error for SOI2 as a function of SNR when DOA of SOI1 is 5°, DOA of SOI2 is 30° and DOA of SNOI is 35° (SNOI is BPSK modulated, cyclostationary signal whose bit rate is 8 Mb/s)

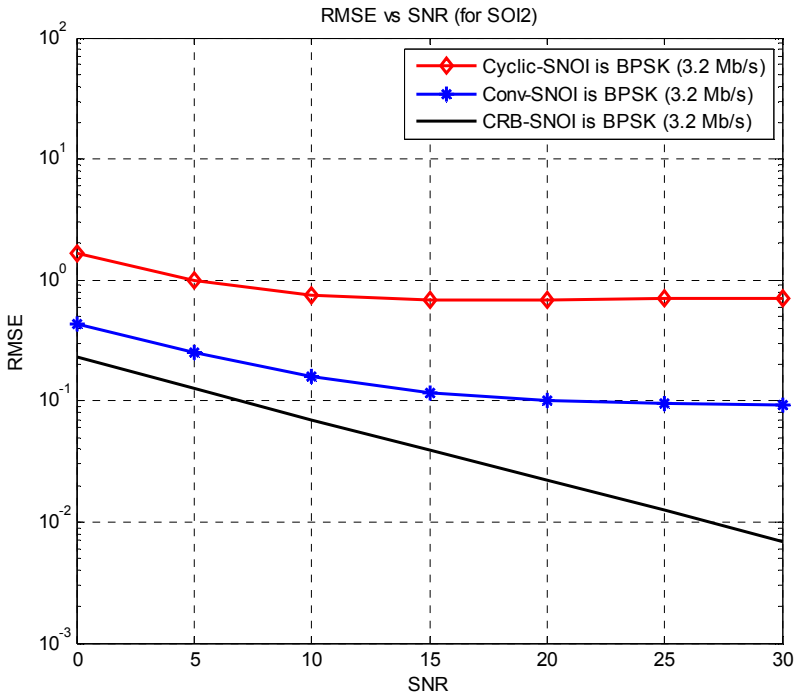

Figure 25 Variation of RMS error for SOI2 as a function of SNR when DOA of SOI1 is 5^o, DOA of SOI2 is 30^o and DOA of SNOI is 35^o (SNOI is BPSK modulated, cyclostationary signal whose bit rate is 3.2 Mb/s)

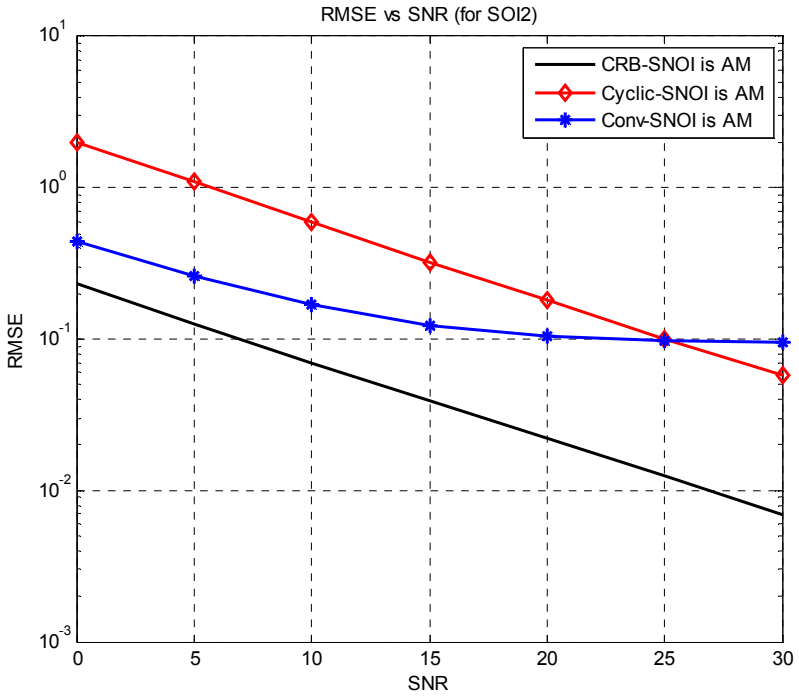

Figure 26 Variation of RMS error for SOI2 as a function of SNR when DOA of SOI1 is 5^o, DOA of SOI2 is 30^o and DOA of SNOI is 35^o (SNOI is AM signal)

Figure 27-Figure 32 are included to show the comparison of Cyclic Root MUSIC and Conventional Root MUSIC algorithms in the existence of a SNOI at 31^o for three different SNOI types. As can be seen from Figure 27-Figure 29, for estimating the DOA of SOI1 Conventional Root MUSIC may be still preferable. However, Figure 30- Figure 32 show that Cyclic Root MUSIC has lower RMSE values for SOI2 than Conventional Root MUSIC when angular separation between SNOI and SOI2 is 1^o. Additionally, for low SNR values Conventional MUSIC fails. Numbers of gross errors for Conventional Root MUSIC among 50 experiments are given in Table 1.

Table 1 Number of Gross Errors for Conventional Root MUSIC Among 50 Experiments for increasing SNR value when DOA of SNOI is 31^o

Scenario \ SNR	0 dB	5 dB	10 dB	15 dB	20 dB	25 dB	30 dB
SNOI is BPSK (8 Mb/s)	39	8	2	-	-	-	-
SNOI is BPSK (3.2 Mb/s)	35	7	1	-	-	-	-
SNOI is AM	37	-	-	-	-	-	-

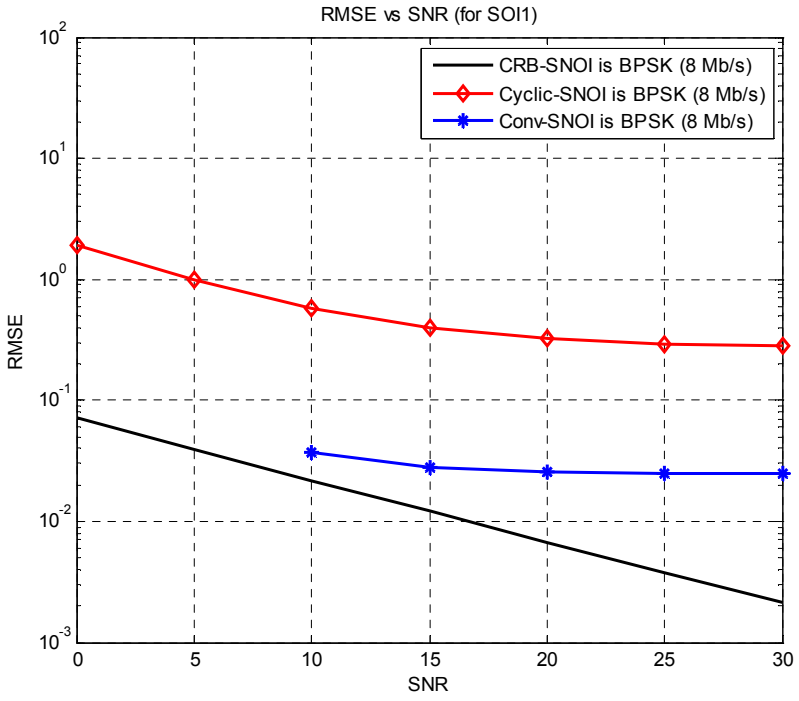

Figure 27 Variation of RMS error for SOI1 as a function of SNR when DOA of SOI1 is 5^o, DOA of SOI2 is 30^o and DOA of SNOI is 31^o (SNOI is BPSK modulated, cyclostationary signal whose bit rate is 8 Mb/s)

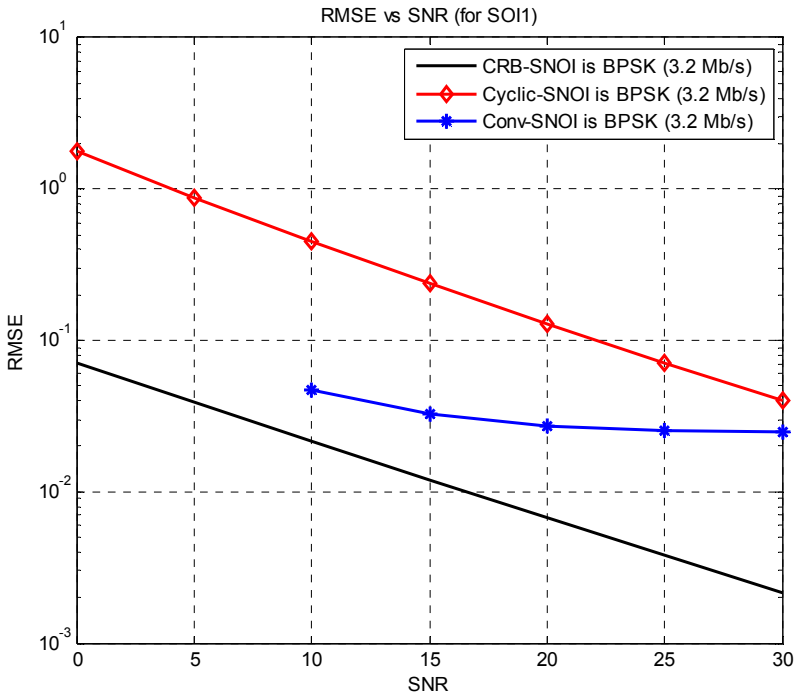

Figure 28 Variation of RMS error for SOI1 as a function of SNR when DOA of SOI1 is 5^o, DOA of SOI2 is 30^o and DOA of SNOI is 31^o (SNOI is BPSK modulated, cyclostationary signal whose bit rate is 3.2 Mb/s)

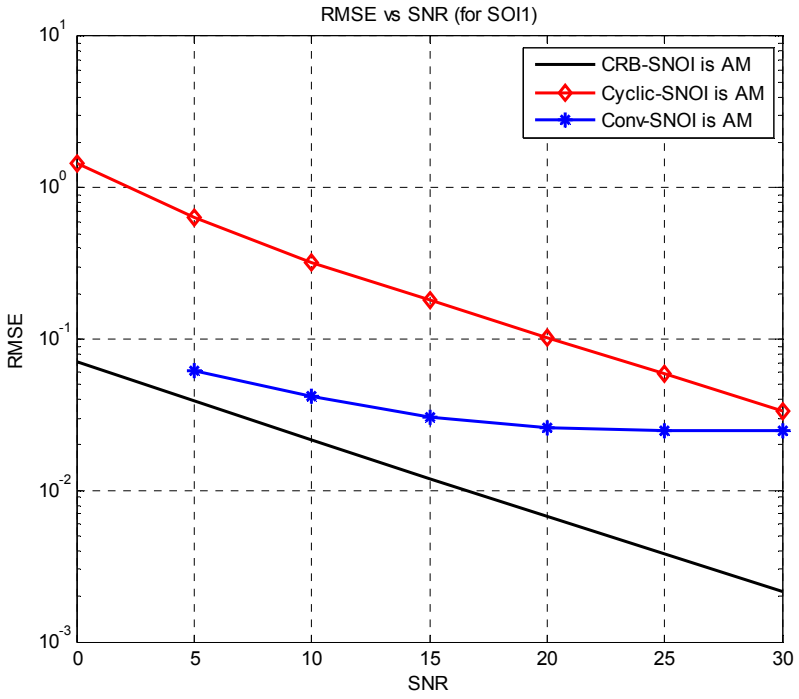

Figure 29 Variation of RMS error for SOI1 as a function of SNR when DOA of SOI1 is 5^o, DOA of SOI2 is 30^o and DOA of SNOI is 31^o (SNOI is AM signal)

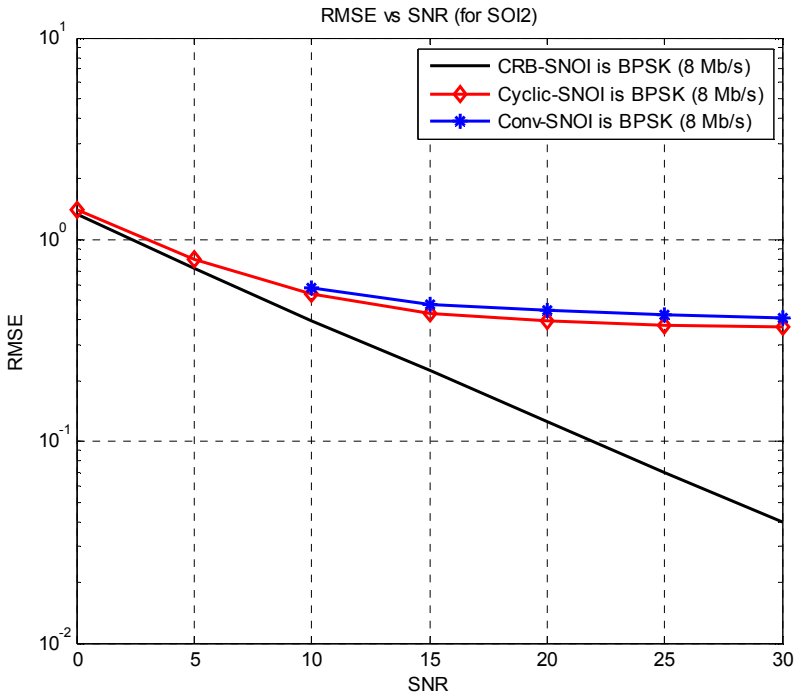

Figure 30 Variation of RMS error for SOI2 as a function of SNR when DOA of SOI1 is 5^o, DOA of SOI2 is 30^o and DOA of SNOI is 31^o (SNOI is BPSK modulated, cyclostationary signal whose bit rate is 8 Mb/s)

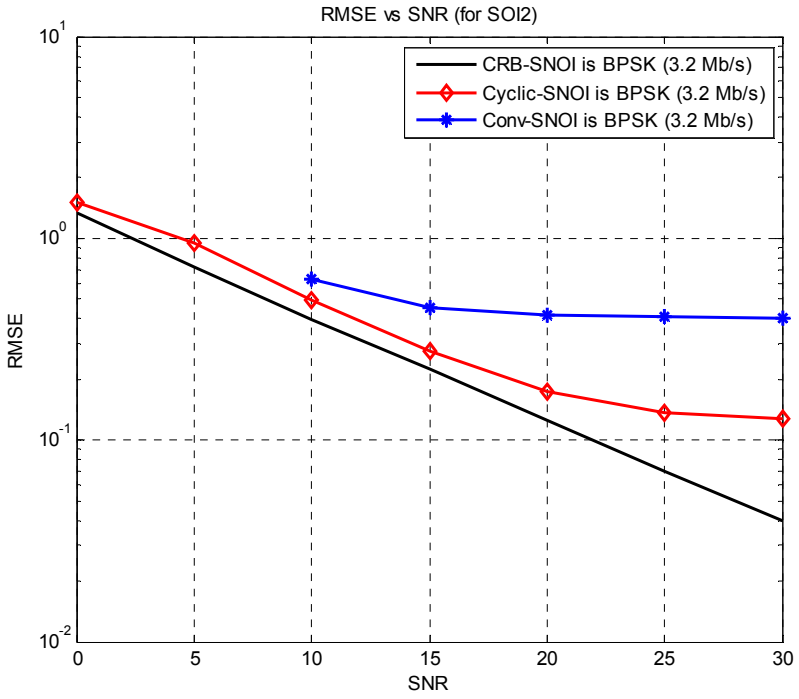

Figure 31 Variation of RMS error for SOI2 as a function of SNR when DOA of SOI1 is 5^o, DOA of SOI2 is 30^o and DOA of SNOI is 31^o (SNOI is BPSK modulated, cyclostationary signal whose bit rate is 3.2 Mb/s)

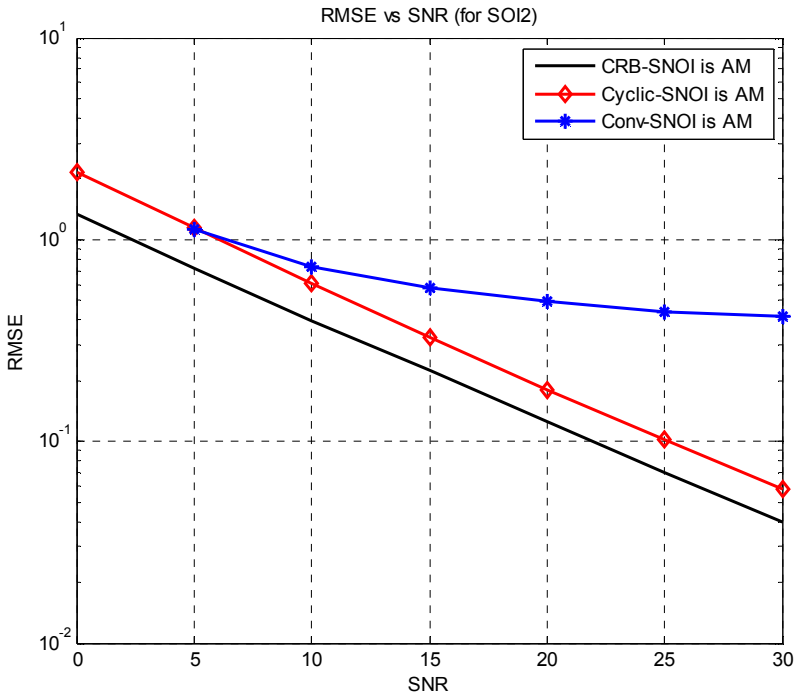

Figure 32 Variation of RMS error for SOI2 as a function of SNR when DOA of SOI1 is 5^o, DOA of SOI2 is 30^o and DOA of SNOI is 31^o (SNOI is AM signal)

Simulation results in this section show that Conventional MUSIC has better performance than Cyclic MUSIC in the signal scenarios which do not contain a SNOI or contain a SNOI that is sufficiently separated from SOI. This result is consistent with the result that is given in [26] which compares the Conventional MUSIC and Cyclic MUSIC algorithms without combining them with spatial smoothing and interpolation methods. In [26], performance of Cyclic MUSIC algorithm is related to a parameter called "feature strength". Feature strength of a signal for a cycle frequency α and a lag τ is defined as $\rho_{xx}^{\alpha}(\tau) = R_{xx}^{\alpha}(\tau)/R_{xx}(0)$. It should be noted that magnitude of feature strength takes a value smaller than 1. For the values of feature strength that are closer to 1, the difference between Cyclic MUSIC and Conventional MUSIC algorithms will be smaller. For the BPSK signal used in the simulations, this value is 1/6. This explains the reason of the difference between Cyclic MUSIC and Conventional MUSIC algorithms for the signal scenarios which do not contain a SNOI or contains a SNOI that is far enough from SOI. However, it is worth to exploit the cyclostationarity properties of the signals if the SNOI is too close to the SOI. Simulation results show that, especially for low

SNR values, Conventional Root MUSIC fails to estimate the DOA of the SOI that is closely placed near the SNOI and in such an environment Cyclic MUSIC continues to work.

Another result that can be concluded from the simulation results is that the RMSE curves of the algorithms do not generally follow the CRB curves. The reason of this difference is shown as the statistical inefficiency of the spatial smoothing and interpolation methods especially for closely spaced signals in [25].

4.3 EFFECT OF SNOI SEPARATION

In this section, performances of Cyclic Root MUSIC and Conventional Root MUSIC are compared while DOA of SNOI is varying around SOI2.

In the following, DOA of SNOI is swept from 24° to 29° and from 31° to 36° with increment 1°. DOA of SOIs are 5^o and 30^o. Total observation duration is considered as 100 μs. Interpolation sector is assumed to be 0^o-45^o with 0.01 step size. Simulation results for two different SNR values are included. In order to exploit the behaviors of the algorithms, first a typical SNR value, specifically SNR=15 dB, is used. Secondly, SNR=0 dB is considered to analyze the behavior of the algorithms under close SNOI and low SNR value cases at the same time. For both SNR values, all three scenarios, which differ in SNOI types, are handled.

In Figure 33-Figure 35, the RMSE values of the DOA estimates of SOI2 as a function of actual DOA of SNOI are given for different scenarios and SNR=15 dB. As expected, RMS errors for Conventional Root MUSIC increase when the separation between SNOI and SOI2 is decreased. Unexpectedly, in Figure 33 and Figure 34, it seems as RMS errors of Cyclic Root MUSIC decrease when the separation between SNOI and SOI2 is decreased. As can be observed from Section 4.1, when SNOI is a BPSK signal, Cyclic Root MUSIC cannot show its signal selectivity property as much as in Amplitude Modulated SNOI scenario. Because of this poor selectivity in BPSK modulated SNOI scenarios, Cyclic Root MUSIC can find the DOA estimates as the values in between the actual DOA values of SOI2 and SNOI. Therefore, when the separation between SNOI and SOI2 is decreased, Cyclic Root MUSIC starts to find closer DOA estimation values to actual DOA of SOI2.

This is the reason of the decrease when the separation between SNOI and SOI2 is small. Such a result is also matched with the simulation results that are given in [26]. Actually, for Cyclic Root MUSIC method the effect of SNOI should be totally eliminated and RMS errors should stay constant. This behavior can only be observed in Amplitude Modulated SNOI scenario as shown in Figure 35.

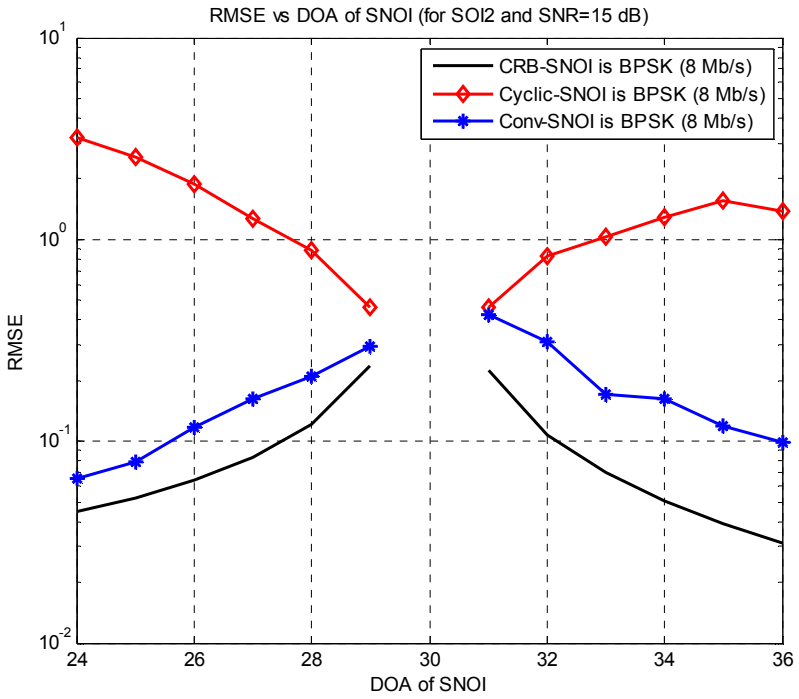

Figure 33 Variation of RMS error for SOI2 when DOA of SNOI is swept around SOI2. Actual DOAs of SOI1 and SOI2 are 5^o and 30^o, respectively. SNR is 15 dB. (SNOI is BPSK modulated, cyclostationary signal whose bit rate is 8 Mb/s)

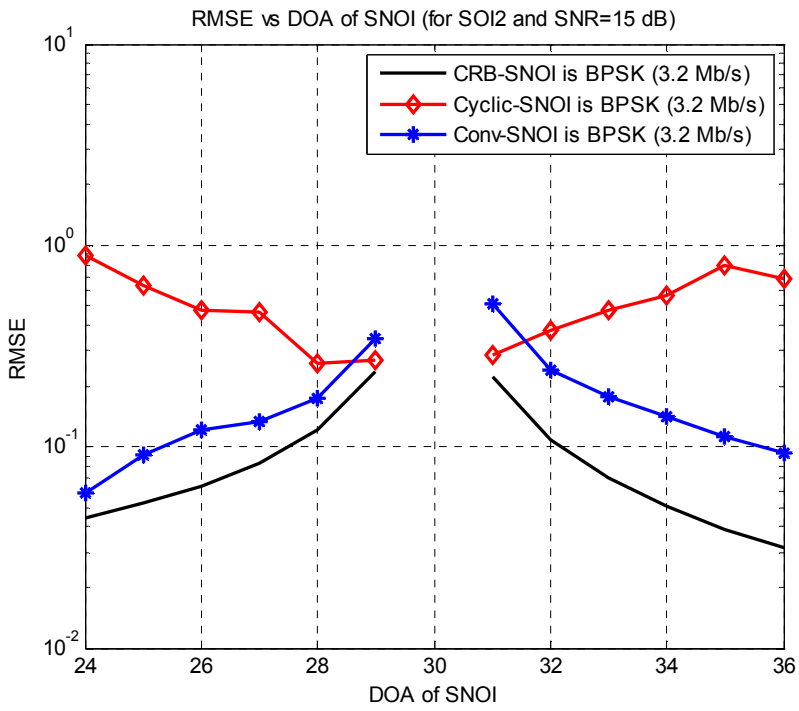

Figure 34 Variation of RMS error for SOI2 when DOA of SNOI is swept around SOI2. Actual DOAs of SOI1 and SOI2 are 5^o and 30^o, respectively. SNR is 15 dB. (SNOI is BPSK modulated, cyclostationary signal whose bit rate is 3.2 Mb/s)

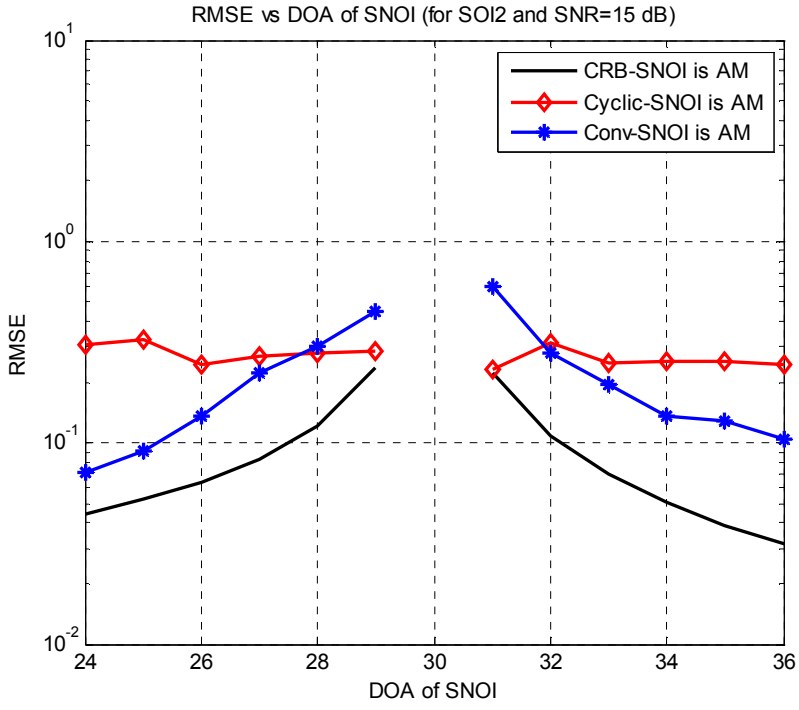

Figure 35 Variation of RMS error for SOI2 when DOA of SNOI is swept around SOI2. Actual DOAs of SOI1 and SOI2 are 5^o and 30^o, respectively. SNR is 15 dB. (SNOI is AM signal)

Figure 36-Figure 38 are included to show the effect of close SNOI and low SNR at the same time. Although RMSE of the Cyclic Root MUSIC is generally higher than that of Conventional Root MUSIC, Conventional Root MUSIC shows gross errors as given in Table 2 when the spatial separation between SNOI and SOI2 is small. As introduced in the beginning of the chapter, Conventional Root MUSIC is assumed to be useless for the values that cause too many gross errors. Therefore these results of Conventional Root MUSIC are not included in the RMSE graphs.

Table 2 Number of Gross Errors for Conventional Root MUSIC Among 50 Experiments for varying DOA value of SNOI when SNR is 0 dB

Scenario \ DOA of SNOI	24	25	26	27	28	29	31	32	33	34	35	36
SNOI is BPSK (8 Mb/s)	-	-	-	-	6	33	26	4	-	-	-	-
SNOI is BPSK (3.2 Mb/s)	-	-	-	2	6	38	26	8	-	-	-	-
SNOI is AM	-	-	-	2	6	21	28	4	-	-	-	-

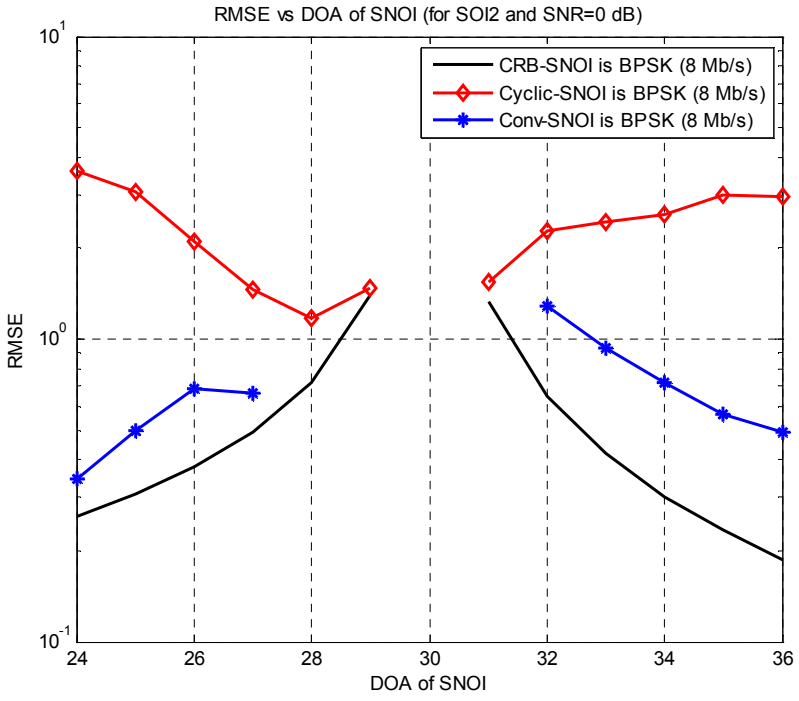

Figure 36 Variation of RMS error for SOI2 when DOA of SNOI is swept around SOI2. Actual DOAs of SOI1 and SOI2 are 5^o and 30^o, respectively. SNR is 0 dB. (SNOI is BPSK modulated, cyclostationary signal whose bit rate is 8 Mb/s)

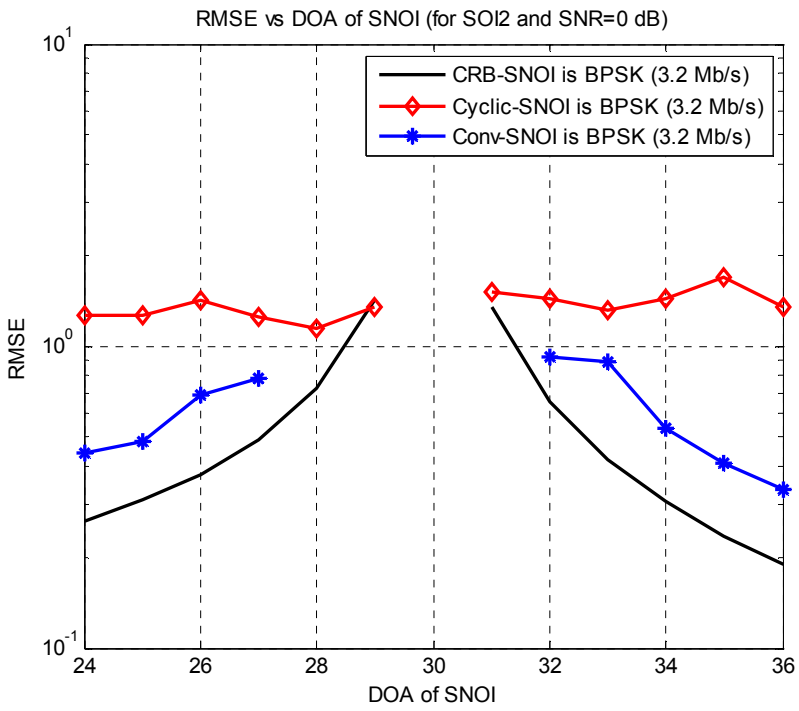

Figure 37 Variation of RMS error for SOI2 when DOA of SNOI is swept around SOI2. Actual DOAs of SOI1 and SOI2 are 5^o and 30^o, respectively. SNR is 0 dB. (SNOI is BPSK modulated, cyclostationary signal whose bit rate is 3.2 Mb / s)

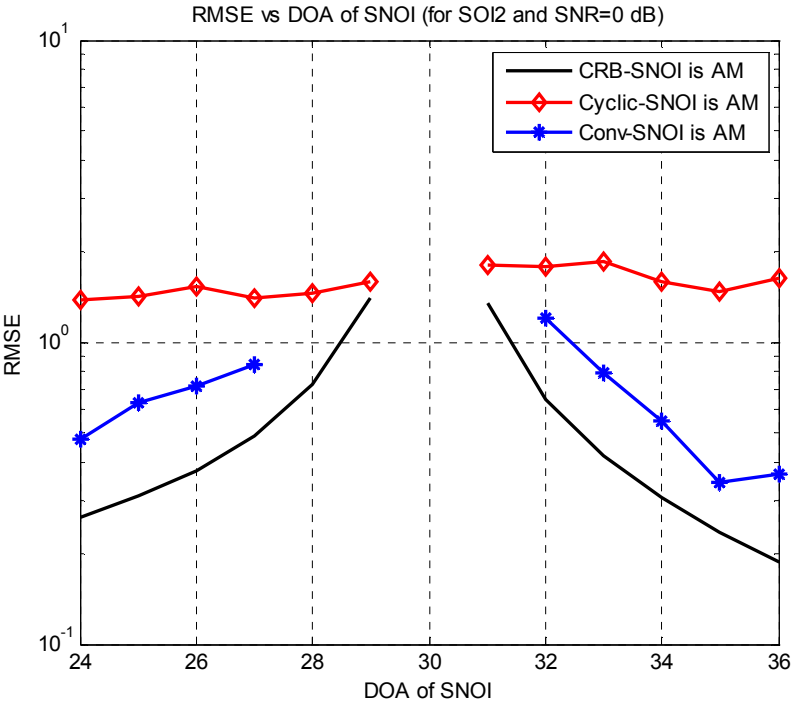

Figure 38 Variation of RMS error for SOI2 when DOA of SNOI is swept around SOI2. Actual DOAs of SOI1 and SOI2 are 5^o and 30^o, respectively. SNR is 0 dB. (SNOI is AM signal)

As a summary, simulation results of this section show that Conventional Root MUSIC has better performance than Cyclic Root MUSIC even in the existence of a SNOI when SNOI is sufficiently separated from SOI2. However, in the existence of a SOI and a SNOI which are spaced closely, Conventional Root MUSIC starts to fail especially under low SNR and Cyclic Root MUSIC can still work.

4.4 EFFECT OF SOI SEPARATION

In this section, performance of Cyclic Root MUSIC and Conventional Root MUSIC are compared while the difference between the DOAs of SOIs is varying.

DOA of SOI1 is swept from 5° to 20° with increment 1°. DOA of SOI2 is kept constant at 30^o. Total observation duration is considered as 100 μs. Interpolation sector is assumed to be 0^o-45^o with 0.01 step size. Simulation results are illustrated for a typical SNR value, specifically SNR=15 dB. Two signal scenarios are handled.

In Figure 39, variation of RMSE under SOI separation effect is given when no SNOI exists. As expected, RMS errors increase when the separation between SOIs is decreased. Conventional Root MUSIC shows better performance than Cyclic Root MUSIC method for all DOA values of SOI1. In Figure 40, variation of RMSE under SOI separation effect is given when an Amplitude Modulated SNOI exists. As can be seen from figures, addition of the SNOI does not affect the performance of Cyclic Root MUSIC while affecting Conventional Root MUSIC considerably. However, Conventional Root MUSIC still provides lower RMSE.

4.5 EFFECT OF TOTAL OBSERVATION DURATION

In this section, performance of Cyclic Root MUSIC and Conventional Root MUSIC are compared under the effect of total observation duration.

Total observation duration is varied as [3.75 6.25 12.5 25 50 100] μs. Total number of snapshots that can be obtained in these durations are [120 200 400 800 1600 3200]. DOA of SOIs are 5^o and 30^o. Interpolation sector is assumed to be 0^o-45^o with 0.01 step size. Simulation results are illustrated for a typical SNR value, specifically SNR=15 dB. Two signal scenarios are handled.

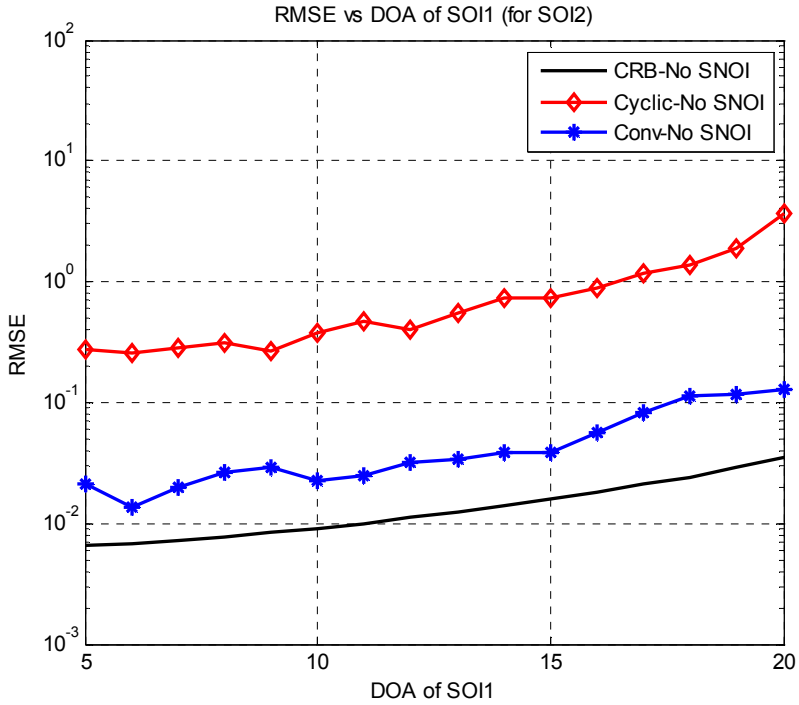

Figure 39 Variation of RMS error for SOI2 when SOI1 is swept from 5° to 20°. DOA of SOI2 is kept as fixed at 30°. (No SNOI exists)

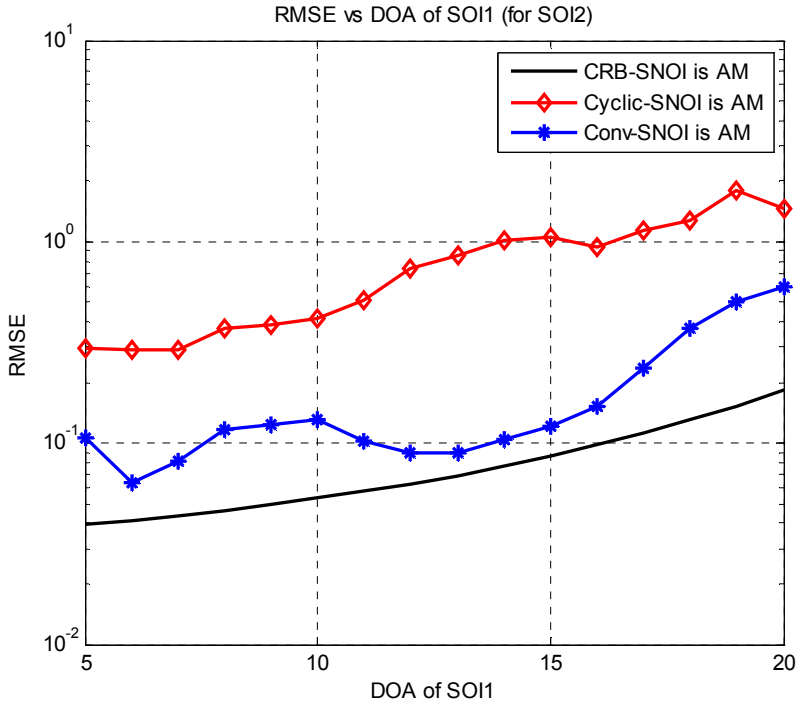

Figure 40 Variation of RMS error for SOI2 when SOI1 is swept from 5° to 20°. DOA of SOI2 and SNOI are kept as fixed at 30° and 35°, respectively. (SNOI is AM signal)

In Figure 41 and Figure 42, variations of RMSE for SOI2 under varying total observation time are given. Figure 41 includes the scenario which does not include SNOI and shows the effect of increasing observation time on RMSE for both algorithms. Figure 42 is included to observe the influence of observation time when an Amplitude Modulated SNOI exists. Expectedly, RMS errors decrease when total observation duration is increased for both algorithms. By inspecting the figures, it is observed that increase of total observation time affects Cyclic Root MUSIC more than Conventional Root MUSIC. RMS errors of Cyclic Root MUSIC decays faster than that of Conventional Root MUSIC under increasing observation duration; the difference of RMSE values from 3.75 μs to 100 μs is 9.82 dB for Cyclic Root MUSIC , whereas RMSE of Conventional Root MUSIC decreases by only 4.58 dB from 3.75 μs to 100 μs .

For Cyclic Root MUSIC algorithm, RMS error decays faster under increasing observation time, since lengthened observation time helps to observe the periodicity of cyclic autocorrelation better. Therefore, keeping the observation time longer is recommended while applying Cyclic Root MUSIC and this requirement may be classified as a disadvantage of the algorithm.

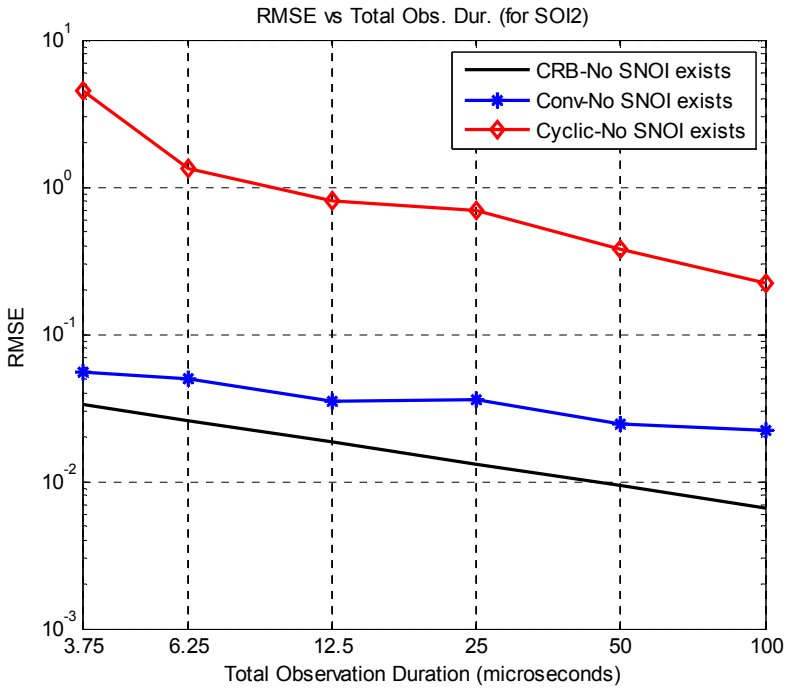

Figure 41 Variation of RMS error for SOI2 as a function of total observation duration when DOA of SOI1 is 5°, DOA of SOI2 is 30° (No SNOI exist)

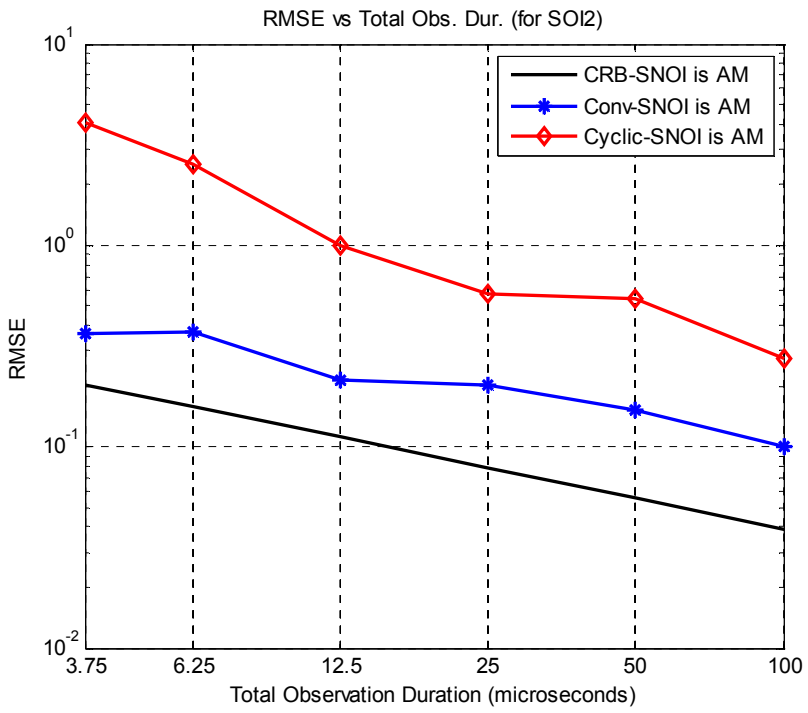

Figure 42 Variation of RMS error for SOI2 as a function of total observation duration when the DOA of SOI1 is 5^{o}, DOA of SOI2 is 30^{o}, DOA of SNOI is 35^{o} (SNOI is AM signal)

4.6 EFFECT OF POWER DIFFERENCE BETWEEN THE SOIs AND SNOI

Effect of power difference between the SOIs and SNOI is analyzed in this section.

Total observation duration is considered as 100 μs. DOAs of SOI1, SOI2, and SNOI are kept constant as 5°, 30°, and 35°, respectively. Interpolation sector is assumed to be 0°-45° with 0.01 step size. Three signal scenarios which differ in SNOI types are used. In the below given simulation results, same power level is set for SOI1 and SNOI. SOI2 is scaled to have 3 dB lower power than SOI1 and SNOI.

In Figure 43-Figure 45, RMS errors for SOI1 and SOI2 are compared for both Cyclic Root MUSIC and Conventional Root MUSIC algorithms for three different SNOI types. As expected, stronger SOI has lower RMS error for both methods. However, RMS errors for SOI1 and SOI2 for Cyclic Root MUSIC are close to each other since Cyclic Root MUSIC tries to eliminate the effect of interferer. This behavior is observed best in Figure 45 for the SNOI is an AM signal that shows weaker cyclostationarity than BPSK modulated ones.

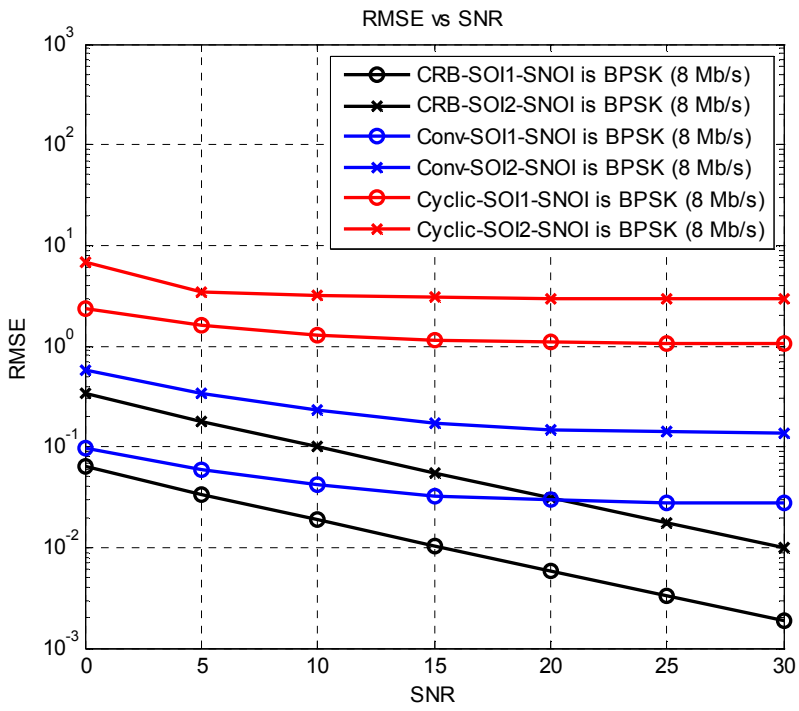

Figure 43 RMS error vs SNR when power of SOI2 is 3 dB lower than that of SOI1 and SNOI. DOAs of SOI1, SOI2 and SNOI are 5^o, 30^o, and 35^o, respectively. (SNOI is BPSK modulated, cyclostationary signal whose bit rate is 8 Mb/s)

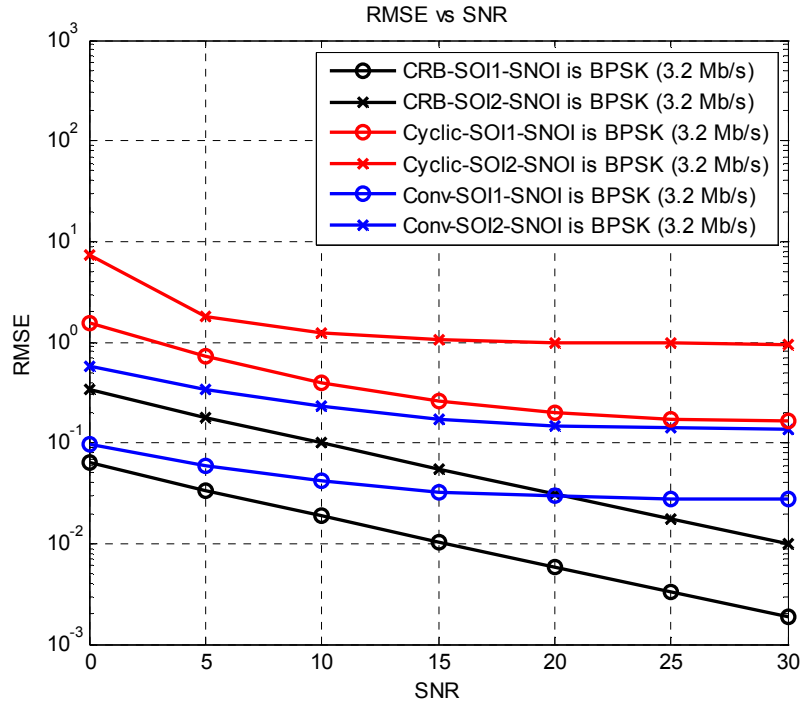

Figure 44 RMS error vs SNR when power of SOI2 is 3 dB lower than that of SOI1 and SNOI. DOAs of SOI1, SOI2 and SNOI are 5^o, 30^o, and 35^o, respectively. (SNOI is BPSK modulated, cyclostationary signal whose bit rate is 3.2 Mb/s)

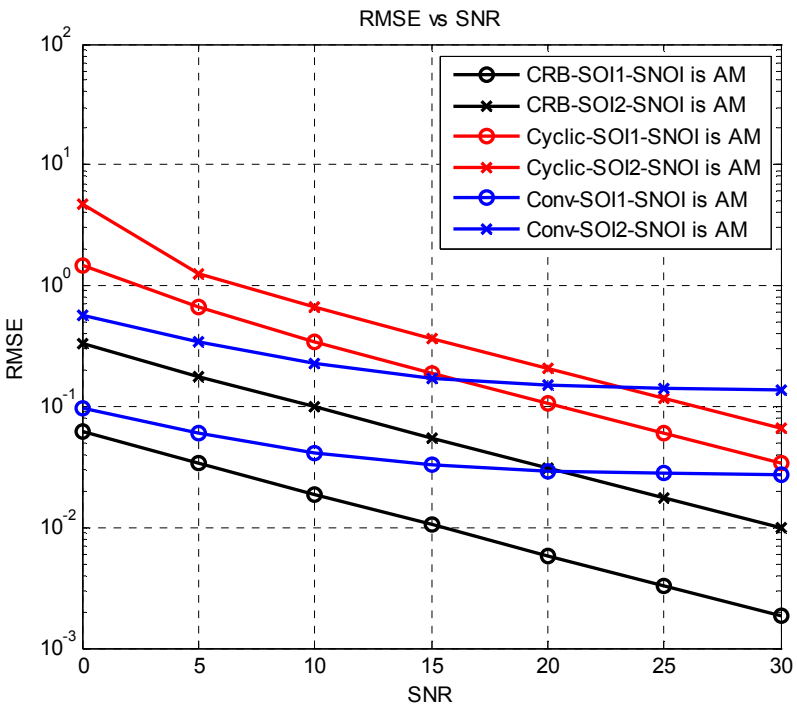

Figure 45 RMS error vs SNR when power of SOI2 is 3 dB lower than that of SOI1 and SNOI. DOAs of SOI1, SOI2 and SNOI are 5^o, 30^o, and 35^o, respectively. (SNOI is AM signal)

From the simulation results of this section, it can be stated that, for the scenarios in which Cyclic Root MUSIC can show its signal selectivity property better (as in Amplitude Modulated SNOI scenario), Cyclic Root MUSIC is recommended against powerful interferers.

CHAPTER 5

CONCLUSION

In this thesis, direction of arrival estimation problem for coherent, cyclostationary signals received via a Uniform Circular Array (UCA) is discussed.

Cyclostationarity is an inherent property of most of the man-made communication signals. Although many conventional statistical signal processing methods treat random signals as if they are statistically stationary, parameters of the most man-made signals encountered in communication, radar and sonar systems do vary periodically with time so these signals can be modeled as cyclostationary processes. This periodic fluctuation in statistics depends on the signal parameters such as carrier frequencies, chip rates, baud rates, etc.

Cyclostationarity based direction finding methods are based on the usage of this property and have some advantages over conventional methods. Instead of using the autocorrelation matrix as in the conventional methods, these algorithms require the estimation of the cyclic autocorrelation matrix.

In this thesis work, first cyclostationarity concept was discussed and basic properties and definitions for cyclostationary signals are given. Then assumptions used for problem formulation are stated, and Conventional Root MUSIC and Cyclic Root MUSIC methods are summarized. Since both the Conventional MUSIC and Cyclic MUSIC methods fail to estimate the direction of arrivals of coherent (fully correlated) signals that are encountered due to multipath propagation, spatial smoothing method is presented. Two types of spatial smoothing is investigated; forward spatial smoothing and forward backward spatial smoothing. Spatial smoothing makes the conventional autocorrelation matrix or the cyclic autocorrelation matrix nonsingular again even the signals are coherent if the numbers

of subarrays are selected appropriately. Then, array interpolation method is presented to generalize the spatial smoothing method to arbitrary array configurations.

In the simulations, Conventional Root MUSIC and Cyclic Root MUSIC methods are compared by combing these methods with interpolation and spatial smoothing techniques. It is considered that coherent, cyclostationary signals were received via a UCA and the RMSE graphs for **S**ignal **o**f **I**nterests are illustrated under the variation of the following factors; interpolation sector, SNR, spatial separation between SOIs or between SOIs and SNOI, total observation duration, power difference between SOIs or between SOIs and SNOI. These effects are investigated for different signal scenarios which could be distinguished with the **S**ignal **n**ot **o**f **I**nterests types. The summary of the results that are obtained from the simulations is given in the following paragraphs.

Conventional Root MUSIC and Cyclic Root MUSIC methods are compared for different interpolation sectors. Although narrower sector selection is also better for Cyclic Root MUSIC, it is observed that Cyclic Root MUSIC shows more robust behavior against sector changes than Conventional Root MUSIC. Since the required criterion for a suitable interpolation sector was obtained experimentally only for conventional methods in the previous researches [23], application of interpolation technique to cyclostationarity based methods is an issue which can further be studied as a future work.

It is observed that performance of Cyclic Root MUSIC highly depends on the cyclostationarity properties of the SNOI. When Amplitude Modulated SNOI is used, better results are obtained.

When two algorithms are compared under varying SNR and varying SNOI separation, it is observed that in the existence of a SOI and a SNOI which are spaced closely, Conventional Root MUSIC starts to fail especially under low SNR and Cyclic Root MUSIC can still work. This result is compatible with the one found in [26] which compares the Cyclic Root MUSIC and Conventional Root MUSIC algorithms without integrating them with spatial smoothing and interpolation methods.

When the effect of angular separation of SNOI is inspected, it is also observed that Conventional Root MUSIC has better performance than Cyclic Root MUSIC when SNOI is sufficiently separated from SOI. To increase the performance of Cyclic Root MUSIC algorithm, some methods are proposed in literature such as "Improved Cyclic MUSIC" and "Conjugate Cyclic MUSIC". In "Improved Cyclic MUSIC" the performance can be improved by properly choosing the frequency for evaluating the steering vector and in "Conjugate Cyclic MUSIC" conjugate cyclic autocorrelation function can be exploited together with cyclic autocorrelation function to further improve the performance of DOA estimation ([8]). Application of these algorithms in conjunction with spatial smoothing and interpolation methods can be a future work to this study.

For Cyclic Root MUSIC algorithm, RMSE decreases faster under increasing observation time, since lengthened observation time helps to observe the periodicity of cyclic autocorrelation better. Therefore, keeping the observation time longer is recommended while applying Cyclic Root MUSIC and this requirement may be classified as a disadvantage of the algorithm.

It is observed that Cyclic Root MUSIC is recommendable against powerful interferers if the SNOI type lets the Cyclic Root MUSIC to show its signal selectivity property better (as in Amplitude Modulated SNOI scenario).

As a conclusion, advantages of Cyclic Root MUSIC against Conventional Root MUSIC can be cited as follows:

- By exploiting the cyclic autocorrelation matrix, effects of interferences (background noise and the Signals not of Interest (SNOIs)) can be eliminated. In other words, these algorithms have signal selective property to separate especially closely spaced signals with different cycle frequencies under low SNR values.
- Cyclic Root MUSIC shows more robust behavior than Conventional Root MUSIC when the interpolation sector is widened.
- It enables to resolve a number of SOIs not exceeding the number of sensors in the presence of virtually unlimited number of unknown SNOIs.

However, the following disadvantages should be taken into account.

- It requires either knowing or measuring frequency parameters, such as carrier frequency or baud rate, to estimate the cyclic autocorrelation matrix.
- Longer observation time for better cyclic autocorrelation measurements is required.
- It is necessary to measure a different correlation matrix for each SOI which has different cyclostationarity properties.
- It has worse performance than Conventional Root MUSIC when SNOI is sufficiently separated from SOI.

REFERENCES

[1]. A. T. Koç, "Direction Finding with a Uniform Circular Array Via Single Snapshot Processing", Ph.D. Dissertation, Middle East Technical University, January 1996.

[2]. H. Krim and M. Viberg, "Two Decades of Array Signal Processing Research", IEEE Signal Processing Magazine, pp. 67-94, July 1996.

[3]. W. A. Gardner, "Simplification of MUSIC and ESPRIT by exploitation of cyclostationarity," Proc. IEEE, vol. 76, pp. 845–847, July 1988.

[4]. G. Xu and T. Kailath, "Direction of arrival estimation via exploitation of cyclostationarity—A combination of temporal and spatial processing," IEEE Trans. Signal Processing, vol. 40, pp. 1775–1786, July 1992.

[5]. S. V. Schell, R. A. Calabreta, W. A. Gardner, and B. G. Agee, "Cyclic MUSIC algorithms for signal-selective DOA estimation," in Proc. IEEE ICASSP, Glasgow, U.K., pp. 2278–2281, May 1989.

[6]. P. Chargé and Y. Wang, "A Root-MUSIC-like direction finding method for cyclostationary signals" in in IEEE ICASSP 2004.

[7]. Chargé, P.; Wang, Y. and Saillard, J., "An Extended Cyclic MUSIC Algorithm", IEEE Trans. Signal Processing, vol. 51, no. 7, July 2003.

[8]. Yan, H.; Fan, H., "Improved Cyclic and Conjugate Cyclic MUSIC", IEEE Sensor Array and Multichannel Signal Processing Workshop, 2004.

[9]. J.E.Evans, J.R.Johnson, and D.F.Sun "Application of advanced signal processing techniques to angle of arrival estimation in ATC navigation and surveillance system," M.I.T. Lincoln Lab., Lexington, MA, Rep. 582, 1982.

[10]. T.J.Shan, M.Wax, and T.Kailath “On spatial smoothing of estimation of coherent signals” IEEE Trans. Acoust., Speech, Signal Processing, vol. ASSP-33, pp. 806-811, Aug. 1985.

[11]. S.U.Pillai, and B.H.Kwon “Forward/backward spatial smoothing techniques for coherent signal identification " IEEE Trans. Acoust., Speech, Signal Processing, vol. 37 , no. 1, pp.8-15, Jan. 1989.

[12]. R. T. Williams, S. Prasad, A. K. Mahalanabis, and L. Sibul, “An improved spatial smoothing technique for bearing estimation in multipath enviroment,” IEEE Trans. on Acoust., Speech Signal Processing, vol. 36, pp. 1361-1375, 1988.

[13]. W. Du and R. L. Kirlin, “Improved spatial smoothing for DOA estimation of coherent signals,” IEEE Trans, Signal Processing, vol. 33, pp. 806-811, 1991.

[14]. B. Friedlander, and A.J. Weiss “Direction finding using spatial smoothing with interpolated arrays " IEEE Trans. on Aerospace and Electronic Systems, vol. 28, no. 2, pp. 574-587, April 1992.

[15]. R.O.Schmidt, “Multiple emitter location and signal parameter estimation” PhD Dissetatation, Stanford University, Stanford, California, 1981.

[16]. G. Phillips, http://www.eee.bham.ac.uk/acs_gr/res/cyclo/cyclo_main.html December 2000.

[17]. Gardner, W., “Exploitation of Spectral Redundancy in Cyclostationary Signals”, IEEE SP Magazine, April 1991.

[18]. Gardner, W., “Spectral Correlation of Modulated Signals: Part I – Analog Modulation”, IEEE Trans. on Communications, vol. 35, no. 6, June 1987.

[19]. Gardner, W., “Spectral Correlation of Modulated Signals: Part II – Digitial Modulation”, IEEE Trans. on Communications, vol. 35, no. 6, June 1987.

[20]. B. D. Rao and K. V. S. Hari, “Performance Analysis of Root-MUSIC”, IEEE Trans. Acoustics Speech and Signal Processing, December 1989.

[21]. A. J. Barabell, “Improving the resolution performance of eigenstructure-based direction-finding algorithms” Acoustics, Speech, and Signal Processing, IEEE International Conference on ICASSP, April 1983, vol. 8, pp. 336 – 339.

[22]. K. V. Mardia, J.T. Kent, and J. M. Bibby, “Multivariate Analysis”, Academic Press, London, 1979.

[23]. Friedlander, B., “Direction finding using an interpolated array”, Acoustics, Speech, and Signal Processing, vol.5, pp. 2951-2954, 1990.

[24]. Friedlander, B.; Weiss, A.J, “Direction finding for wideband signals using an interpolated array”, Signals, Systems and Computers, November 1991.

[25]. Weiss, A.J; Friedlander, B., “Performance Analysis of Spatial Smoothing with Interpolated Arrays”, IEEE Trans. on Signal Processing, vol. 41, pp. 1881-1892, May 1993.

[26]. S. V. Schell, “Performance Analysis of the Cyclic MUSIC of Direction Estimation for Cyclostationary Signals”, IEEE Trans. on Signal Processing, vol. 42, pp. 3043-3050, November 1994.

[27]. Stoica, P.; Larsson, E.; Gershman, A., “Stochastic CRB for Array Processing: A Textbook Derivation”, IEEE Signal Processing Letters, vol. 8, no. 5, May 2001.

[28]. Friedlander, B.; Weiss, A.J, “On the Cramér-Rao Bound for Direction Finding of Correlated Signals”, IEEE Trans. Signal Processing, vol. 41, no. 1, January 1993.

APPENDIX-A

CONDITIONS FOR THE NONSINGULARITY OF THE SPATIALLY SMOOTHED AUTOCORRELATION MATRIX

Sufficient conditions to guarantee the nonsingularity of the spatially smoothed autocorrelation matrix, regardless of the rank of signal autocorrelation matrix are given in [14]. These conditions should be considered while selecting the interpolated arrays for spatial smoothing.

Here, the required condition is only discussed by using conventional autocorrelation matrix. However, below steps can be applied similarly to cyclic autocorrelation matrix too.

Assume that rank of conventional signal autocorrelation function is P.

Recall that $\overline{R_s}$ is an NxN matrix given in (3.40)

$$\overline{R_s} = \frac{1}{L}\sum_{l=1}^{L} D_l R_s D_l^H \tag{A.1}$$

If $\{\beta_n\}_{n=1}^{N}$ are the eigenvalues of R_s (note that only $P \le N$ of the eigenvalues are nonzero) and $\{u_n\}_{n=1}^{N}$ are the corresponding eigenvectors, then (A.1) can be rewritten as

$$\begin{aligned} \overline{R_s} &= \frac{1}{L}\sum_{l=1}^{L} D_l \left(\sum_{n=1}^{P} \beta_n u_n u_n{}^H \right) D_l^H \\ &= \frac{1}{L}\sum_{n=1}^{P} \beta_n \sum_{l=1}^{L} D_l u_n u_n{}^H D_l^H \end{aligned} \tag{A.2}$$

Recalling that D_l is diagonal, a new column vector, namely d_l, which is equal to the main diagonal of D_l, can be defined. Additionally a new diagonal matrix, U_n, which has the elements of $\sqrt{\beta_n}u_n$ on its main diagonal can be defined. Using these definitions, (A.2) can be rewritten as follows:

$$\begin{aligned}\overline{R_s} &= \frac{1}{L}\sum_{n=1}^{P} U_n \left(\sum_{l=1}^{L} d_l d_l^H \right) U_n^H \\ &= \frac{1}{L}\sum_{n=1}^{P} U_n W W^H U_n^H = CC^H\end{aligned} \tag{A.3}$$

where

$$W \triangleq \left[d_1, d_2, \ldots, d_L \right] \tag{A.4}$$

and

$$C \triangleq \left[U_1 W, U_2 W, \ldots, U_P W \right] \tag{A.5}$$

C is an $NxLP$ matrix and if L (the number of interpolated subarrays) is bigger than N and $P \geq 1$, the rank of C will be equal to N. Clearly, rank of $\overline{R_s}$ is equal to rank of C.

As a conclusion, to have a nonsingular $\overline{R_s}$, the subarray number, L, should be bigger than number of impinging signals, N.

APPENDIX-B

COMPUTATION OF THE CRB

A set of equations useful for computing the CRBs on RMSE of the DOA estimates for an array comprising M sensors that receives the N signals emitted by far-field narrowband sources with direction parameters denoted by $\{\theta_1,\ldots,\theta_N\}$ is given in [27] and [28]. It is summarized in the following.

The array output is a vector with the following correlation matrix (3.8):

$$R = AR_s A^H + \sigma^2 I \tag{B.1}$$

The vector of unknown parameters is

$$\eta = \begin{bmatrix} \theta^T & \nu^T & \sigma^T \end{bmatrix} \tag{B.2}$$

where $\theta = \begin{bmatrix} \theta_1 & \ldots & \theta_N \end{bmatrix}^T$ and ν is the $N^2 x 1$ vector made from $\{R_{s,ii}\}$ and $\{\mathrm{Re}(R_{s,ij}), \mathrm{Im}(R_{s,ij}) \text{ for } j > i\}$ and σ^2 is the variance of the noise.

The Fisher information matrix (FIM) for the parameter vector η is given by

$$FIM_{p,k} = T_{obs} Tr\left(\frac{dR}{d\eta_p} R^{-1} \frac{dR}{d\eta_k} R^{-1}\right) \quad \text{for } p,k = 1,\ldots,N+N^2+1 \tag{B.3}$$

where T_{obs} is the number of independent samples obtained during total observation time.

CRB is equal to the inverse of Fisher information matrix.

In the following, T_{obs} is considered as 1. The results for $T_{obs} > 1$ can be obtained by dividing the CRB values by T_{obs}.

As in most applications, both ν and σ are nuisance parameters. Generally, θ block of the FIM is interested.

The following submatrix of the FIM can be derived to calculate the $CRB(\theta)$. Derivation of this close form expression can be found in [27].

$$\begin{aligned} FIM_{\theta\theta} = 2\,\mathrm{Re}\{&(R_s A^H R^{-1} A R_s) \odot (\dot{A}_\theta^H\, R^{-1}\, \dot{A}_\theta)^T \\ &+(R_s A^H R^{-1}\, \dot{A}_\theta) \odot (R_s A^H R^{-1}\, \dot{A}_\theta)^T\} \end{aligned} \tag{B.4}$$

where $\odot$ is element-by-element product,

and where $\dot{A}_\theta$ is defined as follows:

$$\dot{A}_\theta \triangleq \sum_{n=1}^{N} \frac{\partial A}{\partial \theta_n} \tag{B.5}$$

Then, CRB on RMSE of the DOA estimates is

$$CRB(\theta) = (FIM_{\theta\theta})^{-1} = \left\{ 2\,\mathrm{Re}\left\{ (R_s A^H R^{-1} A R_s) \odot (\dot{A}_\theta^H\, P_A^\perp R^{-1}\, \dot{A}_\theta)^T \right\} \right\}^{-1} \tag{B.6}$$

where

$$P_A^\perp = I - A(A^H A)^{-1} A^H \tag{B.7}$$

Following final expression can be obtained by using the relation $P_A^\perp R^{-1} = 1/\sigma^2 P_A^\perp$

$$CRB(\theta) = \frac{\sigma^2}{2} \left\{ \mathrm{Re}\left\{ (R_s A^H R^{-1} A R_s) \odot (\dot{A}_\theta^H\, P_A^\perp\, \dot{A}_\theta)^T \right\} \right\}^{-1} \tag{B.8}$$